A FIBER OPTIC ARRAY FOR THE DETECTION OF SUB-SURFACE CARBON DIOXIDE AT CARBON SEQUESTRATION SITES

by

Benjamin John Soukup

A thesis submitted in partial fulfillment
of the requirements for the degree

of

Master of Science

in

Electrical Engineering

MONTANA STATE UNIVERSTIY
Bozeman, Montana

November, 2014

DEDICATION

This thesis is dedicated to my brother Zachary. It's neither what happens to us nor what we are given which matters most; it's what we choose to build.

ACKNOWLEDGEMENTS

First and foremost I would like to thank Dr. Kevin Repasky, my advisor, for his relentless hard work and dedication in helping me work towards my degree and the completion of this project. Big thanks as well to Dr. John Carlsten for always being able to explain things in a way that I can understand, and for being a continual source of good ideas. Finally, thank you to my mother and father for all their support.

FUNDING ACKNOWLEDGEMENT

This work is supported by the National Energy Technology Laboratory and the Department of Energy Project number DE-FE0001858. However, any opinions, findings, conclusions, or recommendations expressed herein are those of the author's and do not necessarily reflect the views of the DOE.

TABLE OF CONTENTS

LIST OF TABLES

Table Page

LIST OF FIGURES

Figure Page

LIST OF FIGURES - CONTINUED

Figure Page

ABSTRACT

A fiber sensor array for sub-surface CO_2 concentrations measurements was developed for monitoring geologic carbon sequestration sites. The fiber sensor array uses a temperature-tunable distributed feedback (DFB) laser outputting a nominal wavelength of 2.004 μm. Light from this DFB laser is directed to one of the four probes via an in-line 1x4 fiber optic switch. Each of the probes is placed underground and utilizes filters that allow only soil gas to enter the probe. Light from the DFB laser interacts with CO_2 within the probe before being directed back through the switch. The DFB laser is tuned across two CO_2 absorption features where a transmission measurement is made, allowing the CO_2 concentration to be retrieved. This process is repeated for each probe, allowing CO_2 concentration measurements to be made as a function of time for each probe. The fiber sensor array was deployed for fifty-eight days at the Zero Emission Research Technology (ZERT) field site and for a twenty-eight day period at the Kevin Dome geologic carbon sequestration site. Background measurements indicate the instrument can monitor background levels as low as 1,000 parts per million (ppm). During a thirty-four day sub-surface CO_2 release, elevated CO_2 concentrations were readily detected by each of the four probes with values ranging to over 60,000 ppm.

INTRODUCTION

Rise in Atmospheric Carbon Dioxide

The average atmospheric concentration of carbon dioxide CO_2 has been monitored continuously at the Mauna Loa Observatory in Hawaii since 1957.[1,2] The average atmospheric concentration of CO_2 has risen over the past fifty five year observation record from a mean value of 315.97 parts per million (ppm) in 1959 to more than 400 ppm in 2014. Furthermore, the rate of change of the atmospheric concentration of CO_2 has increased from an average value of 0.85 ppm/year between 1960 and1969 and 2.05 ppm/year between 2004 and 2013. Records of CO_2 concentrations from other sites around the globe show similar results.[2]

The increasing level of atmospheric CO2 is due to anthropogenic activity including the burning of fossil fuel and land use changes.[3-5] The CO_2 emission from fossil fuel combustion was 7.9 gigatonnes of carbon (GtC) per year in 2005 while the CO_2 emission from land use changes, mainly clearing of land, was 1.5 GtC per year in 2005.[6] Atmospheric CO_2 is estimated to contribute approximately 63% of the gaseous radiative forcing responsible for anthropogenic climate change. The increasing atmospheric concentration of CO_2 resulting from anthropogenic sources including fossil fuel consumption and land use changes, is causing international concern regarding the effects on the climate system.[7-15] This concern is due to the fact that the earth acts a blackbody radiator at around -20 ^{o}C and emits infrared light, originally absorbed from the sun, in a range of wavelengths from ~ 3-50 μm. This emitted infrared light corresponds directly

with a number of absorption bands for CO_2, specifically at 12 and 14 μm in wavelength. Energy radiated by the earth is being absorbed by atmospheric CO_2 at these wavelengths, and is causing an overall heating of the earth which is in-turn affecting the climate system.

Carbon sequestration[16-21] is one method for mitigating the emission of carbon dioxide from power generation facilities. Carbon sequestration captures the CO_2 at sources such as coal-fired power plants and then injects the CO_2 into geologic formations to minimize the CO_2 emissions into the atmosphere. Furthermore, injection of CO_2 can be used for Enhanced Oil Recovery (EOR), extending the production lifetime of oil wells. A variety of carbon sequestration projects on the commercial scale are under way, including the Sleipner Saline Aquifer Storage Project[22] currently storing CO_2 beneath the North Sea and the Weyburn Project in Canada,[23,24] which is using injected CO_2 for EOR to extend the life of the oil fields. Furthermore, in the United States, seven regional Carbon Sequestration Partnerships[25] are working to develop the science and technology needed for successful and safe carbon sequestration and EOR.

Monitoring instrumentation is one of many areas of technology development needed to ensure both the integrity of carbon sequestration sites and public safety.[26-33] This instrumentation will be needed for both tracking the fate of the CO_2 once it is injected requiring monitoring technology based on seismic detectors, and instrumentation that can be place down monitoring wells, such as pressure and temperature monitors. Furthermore, detection techniques and instrumentation for near-surface monitoring are needed as well for ensuring both carbon sequestration site integrity and public safety. A

variety of monitoring tools and techniques need to be developed to encompass the wide variability in the carbon sequestration sites. One specific group of detection tools currently in development utilize the light from a tunable distributed feedback (DFB) laser to monitor molecular absorption of ambient air, allowing CO_2 concentrations to be found.[34-38] In this thesis, the development and demonstration of a 1 x 4 fiber sensor array operated with a DFB laser for sub-surface monitoring of CO_2 is presented.

The 1 x 4 fiber sensor array utilizes a single DFB laser operating in the continuous wave (cw) mode with a nominal operating wavelength near two microns to make integrated-path differential absorption (IPDA) measurements of sub-surface CO_2 concentration. The light from the DFB laser is directed by a 1 x 4 fiber optic switch to the first of 4 probes that are placed underground. The light interacts with the sub-surface CO_2 and is then directed back through the switch to a transmission detector. The DFB laser is scanned over CO_2 absorption features allowing sub-surface CO_2 concentrations to be retrieved. The fiber optic switch then addresses the second probe and this process is repeated until measurements at all 4 probes have been completed at which point the process is repeated.

The predecessor to this 1 x 4 array was tested in the years prior to the 2012 test of this instrument. The previous instrument did not incorporate a fiber switch and used only a single sub-surface sensor. Four probes were chosen as a tractable means to test the scalability of the system as pertinent for use at commercial or large-scale sequestration sites.

This 1 x 4 sensor array offers a variety of advantages for commercial and scientific use. The send/call geometry of the programming allows the fiber array to be scaled to *N* probes in a cost-effective manner by utilizing a single laser, two detectors, and one fiber optic switch, which are the expensive components, while designing the probes to be low cost. Commercial switches with up to 1 x 50 are available,[39] allowing this technology to scale up to a 1 x 50 array leading to a low-cost sensor array since the cost of each fiber probe is minimal. Comparable point sensor arrays for CO_2 can easily add an order of magnitude in terms of cost for a system of the same size. Furthermore, because the instrument uses all fiber optic components, the sensor can be configured easily for field deployment and is not affected by adverse weather conditions. The system is also designed to run completely autonomously for extended periods of time, and only requires personnel for data retrieval. Finally, even operating with a very low-power DFB laser, and short-length, free-space cells, sub-surface CO_2 fluctuations due to microbial activity can be monitored. Integration of a second DFB laser and a multiplexer could allow for measurements of sub-surface oxygen (O_2) levels, and allow for conclusions to be drawn on changes in soil gas content and its causes.

This thesis is organized as follows. A brief discussion of integrated-path differential absorption (IPDA) spectroscopy is presented in the rest of this section. In section II, a description of a 1 x 4 fiber sensor array is presented. Data from a fifty-eight day field deployment at a controlled subsurface release of CO_2 at the Zero Emission Research Technology (ZERT) field site[40,41] is presented in section III along with data

from the Kevin Dome deployment. Finally, some brief concluding remarks are presented in section IV.

Integrated Path Differential Absorption Spectroscopy

The atmospheric concentration of a molecular species can be related to the transmission of light by considering the optical depth, αL, where α is the absorption per unit length for the molecular species of interest and L is the length the light interacts with the molecular species of interest. It is notable that losses due to scattering are ignored for these sub-surface probes. The optical depth can be related to the molecular line strength, S, and the normalized line shape parameter, $g(\upsilon - \upsilon_0)$, by the relationship[26]

$$\alpha L = Sg(\nu - \nu_0)NP_aL \tag{1}$$

with $N = N_L \frac{296}{T_a}$ is the total number of molecules, N_L = 2.479x10^{19} molecules/(cm atm) is Loschmidt's number, T_a is the temperature in K, and P_a is the partial pressure of the molecule of interest in atm. The number density of the molecules of interest is NP_a whereas the total number density of molecules is NP_T where P_T is the atmospheric pressure in atm. The concentration of molecules of interest is thus

$$C = \frac{NP_a}{NP_T} = \frac{P_a}{P_T} \tag{2}$$

Using Beer's law, which expresses the transmission as a function of the optical depth as $T = e^{-\alpha L}$ for a gas of uniform concentration, and the above two equations, the concentration for the molecular species of interest is[26]

$$C = \frac{-\ln(T)}{Sg(\nu-\nu_0)N_L(\frac{296}{T_a})P_TL} \tag{3}$$

Values for the line strength, S, and normalized line shape parameter, $g(\upsilon - \upsilon_0)$, are tabulated in the HIgh-resolution TRANsmission molecular absorption (HITRAN) database.[42] With measurements of the transmission for a known path length, and known temperature and pressure, a retrieval of the molecular concentration can be completed using eq.(3).

The subsurface concentration of CO_2 can range up to 10,000 ppm depending on soil moisture, temperature, and microbial activity. A plot of the transmission as a function of wavelength is shown in Figure 1 for a path length of L = 1 m with a total atmospheric pressure of P_T = 1 atm, and an ambient temperature of T_a = 288 °K. The solid black line (dashed blue line, dotted red line) represents the transmission spectrum for a 2,000 ppm (10,000 ppm, 60,000 ppm) CO_2 concentration. These values of CO_2 concentration were chosen as representative of the range of sub-surface CO_2 concentrations expected at a geologic sequestration site. The maximum expected absorption for the line centered at 2.004 02 μm for a CO_2 concentration of 2,000 ppm (10,000 ppm, 60,000 ppm) is 2.9% (13.6%, 57.8%). The transmission measured by the instrument, and the resulting calculated CO_2 concentrations will be based around the 2.004 02 μm absorption line. Values for the wavelength, line strength, and line shape parameter for the eight strongest CO_2 absorption features in the 2.001 to 2.005 μm wavelength range are presented in table 1.

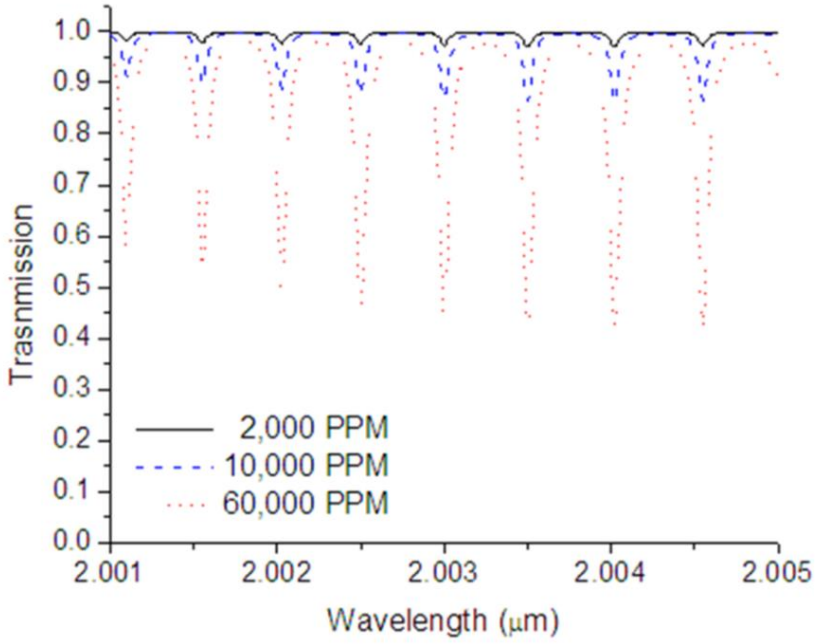

Figure 1 Transmission as a function of wavelength for a 1 m pathlength, a temperature of 288 K, and a pressure of 1 atm. The black solid line (blue dashed line, red dotted line) represents calculations based on a CO_2 concentration of 2,000 ppm (10,000 ppm, 60,000 ppm). This range of CO_2 concentration represents the expected subsurface CO_2 concentration that will be seen at a geologic sequestration site, with background levels typically between 2,000 ppm and 8,000 ppm depending on microbial activity and meteorological conditions.

Wavelength µm	Line strength 10^{-21} cm/molecule	Normalized Line shape cm
2.001 102 0	0.811 2	1.160 0
2.001 557 7	0.931 6	1.151 6
2.002 025 5	1.048	1.140 1
2.002 505 7	1.153	1.130 4
2.002 998 0	1.241	1.116 1
2.003 502 6	1.302	1.102 2
2.004 019 2	1.332	1.084 2
2.004 548 2	1.322	1.0653

Table 1 The wavelength, line strength, and normalized line shape for the eight strongest CO_2 absorption features in the 2.001 µm to 2.005 µm wavelength range. The two absorption lines used in the experiment described in this paper are highlighted.

Differential Error Analysis

In order to gain insight into the accuracy of the instrument a differential error calculation on the concentration calculation was performed. It is apparent from equation (3) the concentration is dependent on a number of constants but three main variables: the temperature, the pressure and the measured transmission. The pressure was not specifically monitored by this instrument, but during field deployment a separate weather station run by the Optical Remote Sensor Laboratory did take constant meteorological measurements.[43] These measurements show that the average pressure varied only by several millibars within any given 24-hour period. During the month of July, 2012 (month of field deployment at ZERT site), the average pressure was 850.8 mb, with maximum and minimum measured pressures at 858 mb and 841 mb, respectively. In

order to calculate the effect of this change on the calculated concentrations of $CO_{2,}$ a differential calculation is made on equation (3) based on the pressure $P_{T,}$ becoming

$$dC = \frac{-\ln(T) * dP_T}{Sg(\nu - \nu_0) N_L (\frac{296}{T_a}) P_T^2 L} \quad (4)$$

Due to the error in the transmission measurement and its large effect on the calculated concentration this error from the pressure is taken to be negligible, and the pressure in the concentration calculation is set to a constant 850mb.

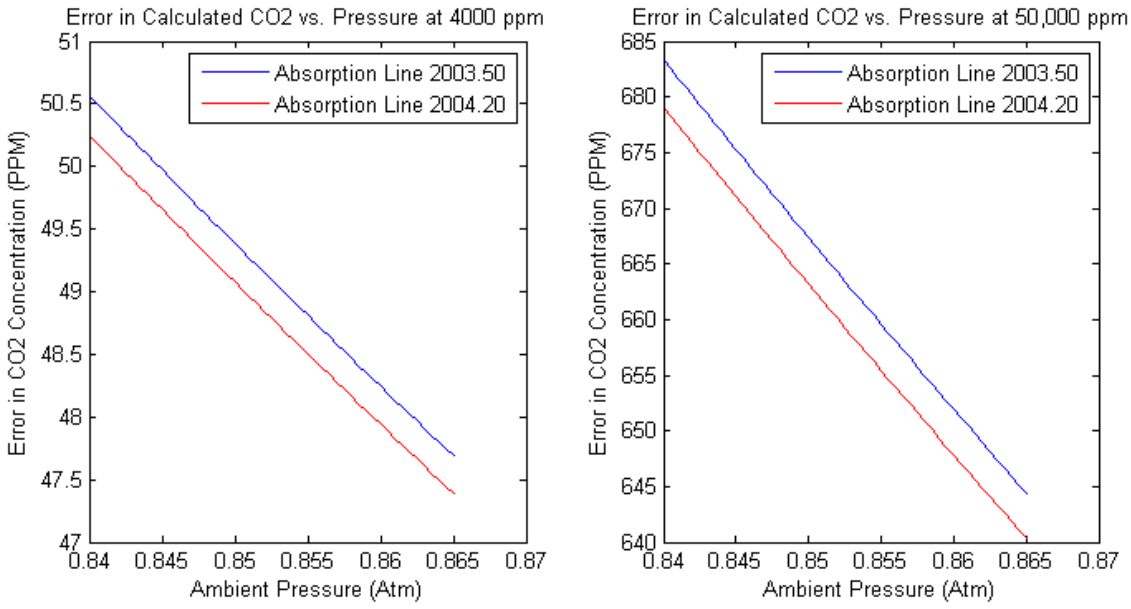

Figure 2 Plots of the error introduced into the concentration calculation from a 10 mb pressure error. The plot on the left is the error from a calculated concentration of 4000 ppm or a transmission of ~95%. The plot on the right is for a concentration of 50,000 ppm or ~50% transmission signal.

The temperature at the probes was monitored by a 10k thermistor wired into the nose of probe 3. The temperature at the probes stayed relatively constant at their buried depth of ~1m. Over the entire month of July 2012, the average subsurface temperature was around 290 K, with a variation of less than ±3K. For each scan then, taking only

minutes, the variation in temperature was far less than 1 K, so the temperature was taken as a constant for each individual probe scan before being inserted into the concentration calculation. It follows that the error from the temperature based on this slight variation is negligible. Equation 5 shows the differential error of the concentration based on temperature.

$$dC = \frac{-\ln(T) * dT_a}{Sg(\nu - \nu_0) N_L (296) P_T L} \tag{5}$$

This error is independent of the actual ambient temperature, but has dependence only on the error in measured temperature (a constant) and the transmission (assuming already that the error from pressure is also negligible).

As mentioned, the greatest error in the concentration came from the error in the transmission. The differential error for transmission derived from equation (3) becomes

$$dC = \frac{dT}{T * Sg(\nu - \nu_0) N_L (\frac{296}{T_a}) P_T L} \tag{6}$$

To simplify this, the differential error for the transmission was taken to be constant for each fiber probe based on its peak transmission signal as this number varied from probe to probe. The normalized transmission errors for probes 1-4 are 3%, 7%, 5%, and 5% respectively. These variations constitute random fluctuations in the measured transmission voltage on the detector at no more than 5 mV. Figures 3 and 4 show the error introduced from the subsurface temperature measurement and the error introduced from the transmission signal measurement, respectively.

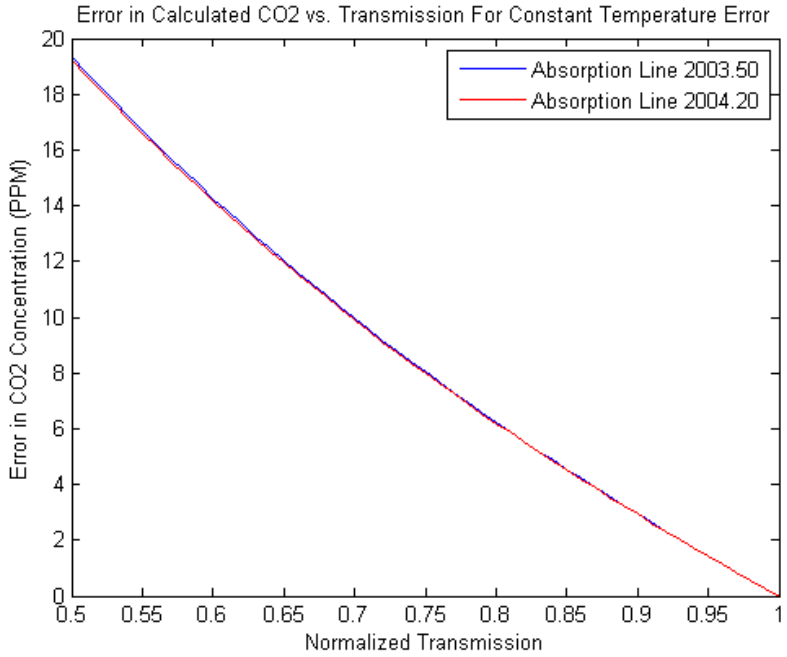

Figure 3 Plot of the error introduced from the temperature for the sub-surface probes for a range of transmission values corresponding to a range of CO_2 concentrations.

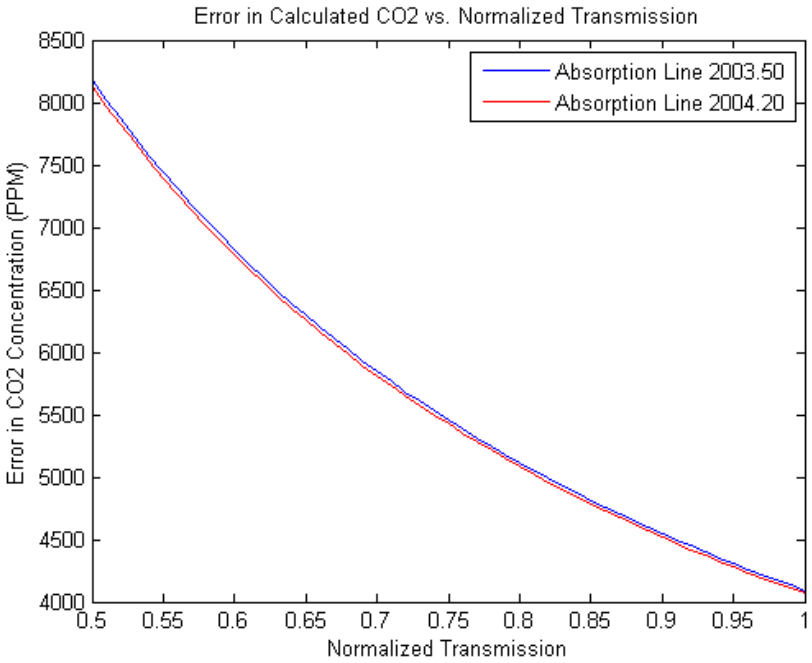

Figure 4 Plot of the error introduced in the concentration calculation from the measured error in the transmission signal at a constant value of 5%. This error is approximately a factor of 10 or higher than the error from temperature and pressure.

THE 2μm SUB-SURFACE FIBER ARRAY

Laser Diode Characteristics

The laser diode used in this instrument is a Nanoplus 2004nm, Fiber-coupled, DFB laser. This laser source was originally used in the predecessor of the 1 x 4 fiber sensor array, and did display characteristics of degeneration over repeated use which will be discussed in more detail in following section on optical power. Table 2 shows some of the specified characteristics of the laser diode.

Parameter	Symbol	Unit	Min	Typical	Max
Wavelength	λ	nm	2003	2004	2005
Optical Power	P_{opt}	mW	-	1	-
Operation Temperature	T	^{o}C	25	35	40
Temperature Tuning Rate	C_T	nm/K	.18	.20	.22
Threshold Current	I_{th}	mA	20	25	50

Table 2 Given characteristics of the 2004um DFB laser.

Temperature Tuning

The operating principle of this instrument relies on wavelength tuning of the DFB over selected molecular absorption features of the CO_2 molecule. This tuning was accomplished using a constant current while tuning the temperature over a range of about 33-39 ^{o}C. This corresponded to a wavelength range of 2003.15 μm to 2004.25 μm which

encompassed the two selected absorption features discussed in the previous section. Each wavelength scan then covered 1.1 nm with 100 steps, thus giving a wavelength step size of 0.011 nm. Exactly why these wavelengths were chosen involved the use of the laser controller and the associated digital-to-analog converter (DAC) card and will be discussed in more detail in the programming section.

Laser Control

The laser temperature and current were regulated using a Wavelength Electronics dual laser driver and TEC controller (LDTC0520). This unit has the option for both onboard and remote control capability. The laser current was run at a constant 60mA using an onboard trimpot. The laser temperature was controlled remotely by the computer for tuning over the desired range. This operation requires a DAC to convert the digital program commands to analog voltage signals for input into the temperature controller. The actual temperature of the laser was monitored in real time with feedback from the built-in laser thermistor. Before field deployment, the laser wavelength was calibrated to specific temperatures. Based on this calibration, the temperature was scanned through a range of temperatures containing the absorption features of interest. In this way the actual TEC temperature, and thus the laser wavelength, can be monitored and controlled from a single panel in the Labview control program.

One issue with the highly compact and portable LDTC0520 was lack of an interlock between the laser anode and cathode when the unit was off. This is of concern for a field-deployed instrument, as power outages or other errors were common. To solve

this problem, a printed circuit board (PCB) was manufactured, utilizing a relay switch to allow for an interlock in laser control. The original power plug was rerouted into this PCB, to which the LDTC0520 was mounted and otherwise functioned as normal. When the system is powered down, intentionally or not, a short between the anode and cathode is achieved and no potential damage from static build up can occur. A schematic of the relay circuit and the mounted LDTC0520 can be seen in Figures 5 and 6.

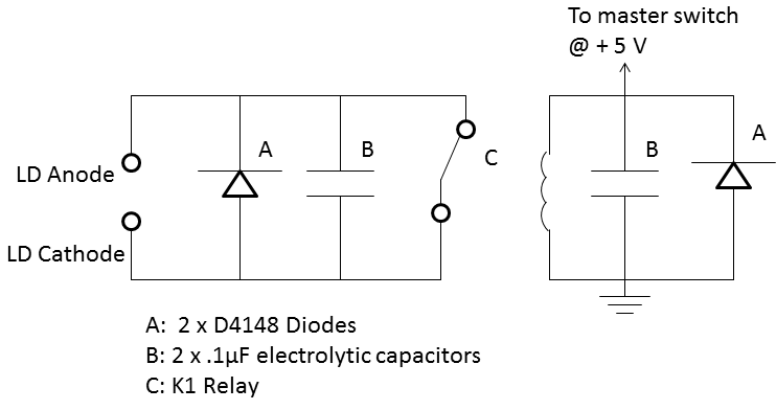

Figure 5 Schematic of the relay circuit used for the laser node shorting/laser protection during power outages.

Figure 6 Image of the LDTC0520 mounted on the relay circuit PCB.

During field deployment, very little change in wavelength was observed in laser operation. Minor shifts were expected to occur in the laser output wavelength due to age or extreme environmental temperature changes, but these effects were minimally observed. Any slight change in the temperature-wavelength correlation of the laser was mitigated by the analysis programming, which always seeks out the minima of the returned intensity and assigns it to the proper absorption feature (by wavelength). Long-term study of the change in laser wavelength due to extended use would be useful for further understanding of system performance.

Detectors

For both the transmission and reference detectors, two New Focus model 2034 IR InGaAs photoreceivers were used. At the 2μm wavelength used, the responsivity of the detectors is approximately 1A/W with a transimpedance gain of $2x10^3$V/A on the low gain setting.

Any voltage measured by the detectors from the laser can be converted into an optical power by the equation:

$$P_{in} = {}^{V}/_{(RG)} \tag{7}$$

where P_{in} is the optical power, V is the measured voltage on the detectors, R is the responsivity, and G is the transimpedance gain for the detector.

Optical Power

The typical voltage of the 14-pin laser diode directly out of the connecting fiber was 630 mV, which corresponds to a power of 315 μW out of the laser. The specified optical power for the DFB operating at ~25 ^{o}C or 10kΩ is 1 mW. It is expected that at a higher operating temperature, the output optical power would decrease. It is of note that over the course of several years the output power dropped considerably from around 0.5 mW. It is likely that the change in optical power of the laser diode was the result of deformations or cracks in the laser cavity, possibly due to the repeated stress of temperature tuning and the fluctuations of the operating temperature during field deployment in previous years. The resulting laser output, regardless of its denigration in power, was still stable in wavelength and power (at a given temperature) and could still be utilized for the field deployment.

System Layout

A schematic of the fiber sensor array is shown in Figure 7. A distributed feedback (DFB) laser operating at 2.004 μm was mounted in a 14 pin butterfly package with a fiber pigtailed output. The DFB laser is a continuous wave (CW), tunable source that has an internal thermoelectric cooler (TEC) that allows temperature tuning of the DFB laser. The DFB laser is mounted in a commercial mount from ILX Lightwave that provides a second TEC that is used to stabilize the ambient temperature in which the DFB laser operates. This second TEC is important during field operations where temperatures can range between a low of 0 °C at night to a high of 35 °C during the day.

The fiber-coupled output from the DFB laser is non-isolated and directly incident on an in-line fiber splitter, which uses 62.5µm multi-mode optical fiber, with 50% of the light from one port directed to a reference detector. The remaining 50% of the light from the second port is directed to an in-line 1 x 4 fiber optic switch. The in-line opto-mechanical fiber optic switch has an insertion loss of less than 0.6 dB with a cross talk of less than -60dB. Each of the four fiber-coupled output ports is connected via a multi-mode fiber optic cable to a probe that is placed into the ground. The fiber optic cables are all 62.5µm, FC/PC multimode fibers approximately three meters in length. At the probes the light is collimated and allowed to interact with the CO_2 that diffuses into the buried probes through Millipore filters placed at the top and bottom of the probes. These filters allow the soil gas to diffuse into the probes but keep out dirt and water. The light is then re-coupled into the multi-mode optical fiber where it is directed back through the fiber optic switch and is again incident on the in-line fiber splitter where light from one port is directed to a transmission detector. The reference and transmission detectors are monitored using a multichannel voltmeter that can be read by a computer via a GPIB interface.

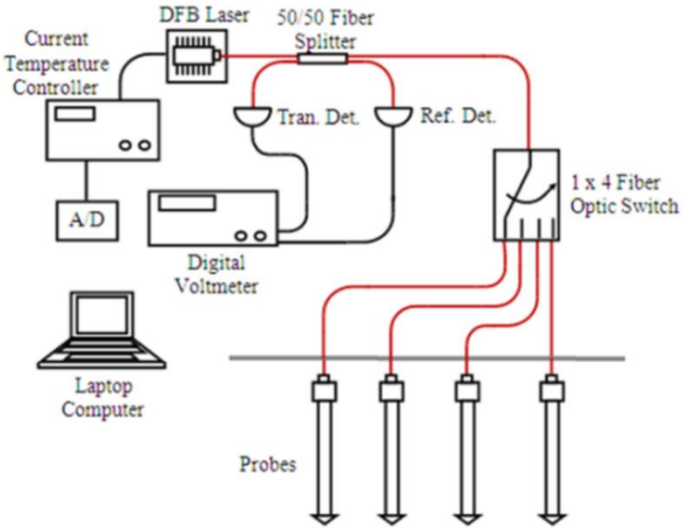

Figure 7 Schematic of the 1 x 4 fiber sensor array.

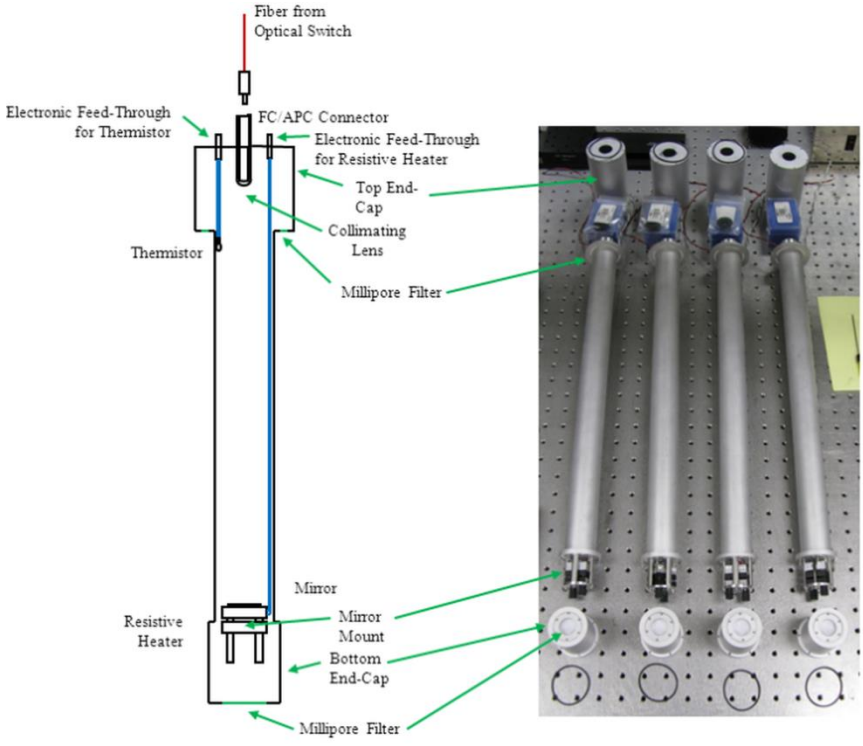

Figure 8 Schematic of the fiber probe is shown on the left and four completed fiber probes shown on the right.

The Subsurface Probes

A schematic of the fiber probes is shown in Figure 8. The optical fiber from the 1 x 4 fiber optic switch is a multi-mode optical fiber with a core diameter of 62.5 μm (Optequip A20134) with angled physical contact (FC/APC) connector. This connector couples to the fiber probe via a keyed FC/APC connector mounted in the top-end cap of the probe. The light exiting the fiber is collimated with an aspheric, fiber coupled, collimator which has a focal length of f = 11 mm and a reflectivity of <3%. The collimated light travels to the mirror mounted in a commercial optical mount that reflects the light back through the collimating lens and back into the optical fiber. The mirror mount has a resistive heater attached to ensure that condensation does not form on the mirror when the fiber probe is buried for extended periods of time. A thermistor is also placed in the fiber optic probe to allow temperature measurements needed for the data inversion discussed in section II. Millipore filters in both the top end cap and bottom end cap allow soil gas to move into and out of the fiber probe when the fiber is buried while keeping out dirt and water. The overall length of the fiber probe is 60 cm with a 50 cm free space path length where the light and CO_2 can interact. The diameter of the end caps are 5.0 cm while the diameter of the narrower central tube is 3.8 cm. The fiber probes are made out of aluminum and were machined by the author. A picture of the four completed probes is shown in Figure 8. During field deployment each of the four probes was buried in large diameter PVC tube that had been perforated with 3/16 inch holes to allow for soil gas to pass through the tube unimpeded. This was done to allow for easy access to the probes once buried. In the event the return signal was lost the probes could

easily be removed from the ground for inspection and maintenance. However, during field testing, the probes did not require removal once placed in the ground. Originally the probes were also designed with piezo-electric transducers mounted behind the mirror to help peak up the return signal after an undesired strain or stress on the probe caused some loss in return intensity. Once it was realized that the fiber probes remained at peak signal for long durations of time, the piezos were removed from the system.

Programming and Instrument Control

The instrument is operated using software developed in the Labview programming environment. Data is collected in the following manner**.** Once the channel to the desired probe is set the programming begins a digital ramp to slowly tune the laser by stepping its operating temperature. This is a basic positive ramp function that outputs a voltage to a DAC in which the user can set the step size and start/stop values of the function. At each step of the voltage ramp the DAC converts the value to its analog counterpart and outputs it to the laser TEC controller. This, in turn, causes small positive change in temperature for the diode and thus a small increase in wavelength. During each step of the temperature, the computer records a reference signal value (voltage) from the laser, a transmission signal from the probe, and the subsurface temperature. The reference and transmission signals are actually recorded several times per step and the median value is recorded for that temperature (wavelength) step. This is done to help mitigate any noise or modulation while the laser stabilizes to that temperature. The dwell time at each step, the step size, and the time between each reference and transmission

measurement are all defined by the user. Experimental measurements show that the laser requires at least one second to settle into each temperature and stabilize the output wavelength. During the actual field testing of the instrument each temperature step took about four seconds allowing ample time for the laser wavelength to stabilize and the computer to monitor accurately the reference and transmission signal. Figure 9 shows a simplified block diagram of the system programming scheme.

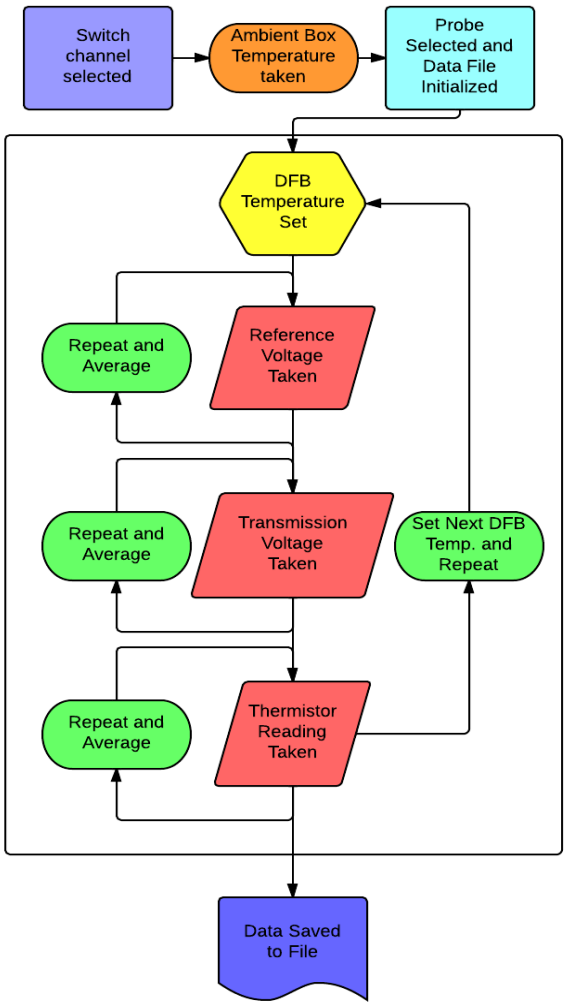

Figure 9 Chart demonstrating the flow of data collection for the fiber array in the Labview programming.

As was discussed in the section on temperature tuning, the laser is tuned between 2003.15 μm to 2004.25 μm. This range was selected for a very specific set of reasons. The DFB contained a built-in 10k thermistor for feedback on the laser temperature set by the TEC. The LDTC0520 utilized a voltage input, from 0 -1 V that corresponded to a specific temperature on the TEC. Thus the tuning wavelength needed to be converted to a temperature, which could be converted to a resistance in kΩ on the TEC, and finally converted to a voltage for input into the LDTC0520 via the Labview programming. The approximate start-stop wavelengths corresponded to a temperature range of 33 -39 ^{o}C, measured by the Bristol wavelength meter. Figure 6 shows the relationship between the DFB set temperature and the set resistance in kΩ. The nearest whole-number values for the TEC resistance that captured the desired absorption features fell between 7-5.5kΩ; this resistance range gives the exact wavelength tuning range from 2003.15 to 2004.25 μm. As mentioned, the LDTC0520 utilized a voltage input. To convert the TEC set resistance to a voltage, a simple conversion is done using the bias current on the feedback sensor, in this case, a 100 μA thermistor. The input voltage on the LDTC0520 ranged from 0-2 V; this, combined with a 12-bit DAC card ranging from 0-5 V, meant that the minimum voltage resolution was approximately 1.2 mV. Using 100 steps between the selected voltage range of 0.7-0.55 V for input meant the system would have 1.5V/step, just above the DAC voltage resolution and enough points per scan to clearly define any absorption features.

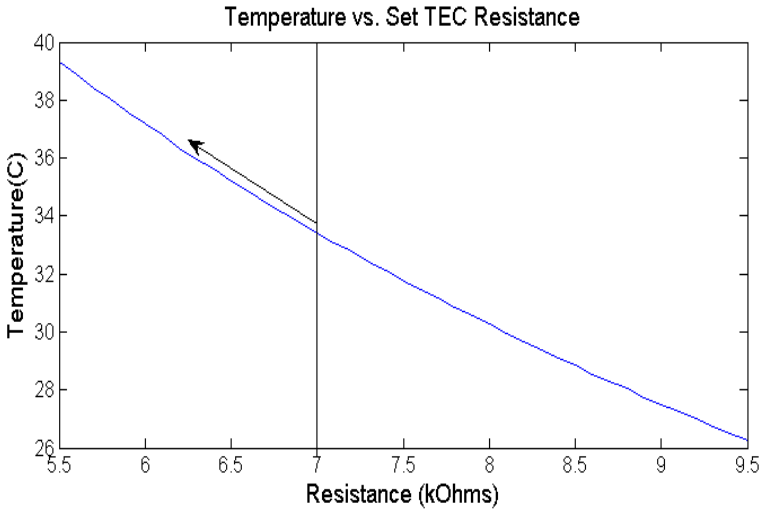

Figure 10 A plot of the actual DFB temperature versus the TEC set point in kΩ. The black vertical line indicates the start of the selected temperature scan range at 7 kΩ scanning down to 5.5 kΩ or about 39.3 ^{o}C laser temperature.

A single scan for a probe takes about seven minutes, contains 100 points of measurement for the reference/transmission signals (mean values), and moves the laser through a temperature range of 33.42-39.33^{o} C. Once a scan is completed, the transmission is normalized and the molecular concentration can be calculated using the results discussed in section I, and the program moves on to the next probe to repeat the entire process.

INSTRUMENT DEPLOYMENT AND FIELD TESTING

The ZERT Site Deployment 2012

The Zero Emissions Research and Technology (ZERT) field site[35,36] is a controlled CO_2 release facility located on the western edge of Montana State University (MSU) in Bozeman, MT (45°39'N, 111°04'W) at an elevation of 1,495 m. The ZERT site has a buried horizontal release pipe that was developed to simulate a longitudinal CO_2 leak source, such as a geologic fault or a weakness in a geologic capstone atop a subsurface reservoir, for the development and testing of near-surface and surface monitoring tools for carbon sequestration. The site is on a relatively flat alluvial plain that consists of thick sandy gravel deposits overtopped by several meters of silts, clays, and topsoil. The buried release pipe is 98 m long, with an inner diameter of 10.16 cm, and is oriented 45° east of true north. The central 70 m of the pipe is perforated to seep CO_2 during injection. A series of eight packers were placed within the release pipe to assist in dispersing the gas evenly along the slotted portions of the release pipe with each of the eight sections of pipe plumbed with its own flow controller. The pipe was buried using a horizontal drilling technique that minimized disturbance to the surface environment; however, the pipe installation was deflected from a perfectly straight path because of cobble in the gravel layer underground.

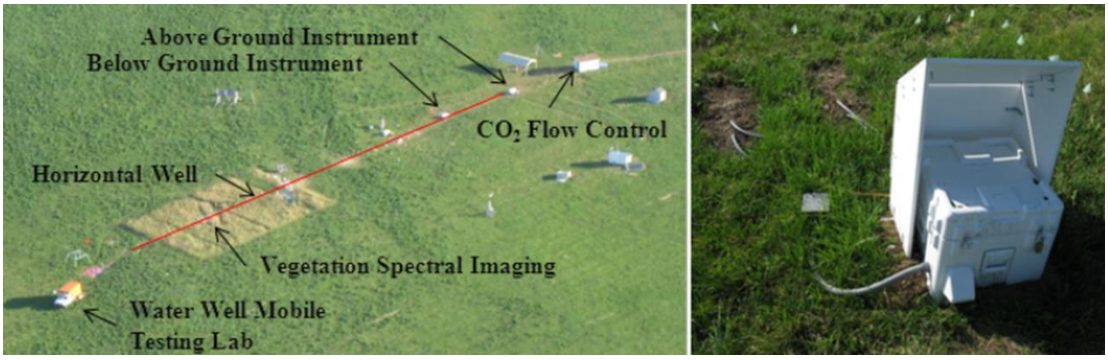

Figure 11 The ZERT field site is shown in the left hand figure with the subsurface pipe location and below ground fiber instrument locations marked. The fiber sensor probe deployed at the ZERT site is shown in the right hand figure.

A thirty-four-day release experiment was performed beginning July 10, 2012. The CO_2 release rate for this experiment was 0.15 tons CO_2/day, about the equivalent to two idling cars, evenly distributed over the eight sections of the underground pipe. The flow rate was chosen in the following manner. Approximately 4 x 10^6 tones CO_2/year can be captured from a 500 MW fossil fuel burning power plant. Over a 50 year period, this would result in a total of 200x10^6 tones CO_2 which could be sequestered. Assuming that the injection area is approximately 1% of a typical geologic fault in size, the flow rate was chosen so that the seepage would mimic less than 0.01% through a typical fault. This implies that the flow rate chosen mimics the levels that need to be monitored and observed at geologic sequestration sites.

Data Collection

A plot of the normalized transmission as a function of wavelength is shown in Figure 12. The solid red line represents the normalized transmission measured using one of the four probes during the release experiment. The Labview program used to collect

and process the data, which was described in section II above, returned a CO_2 concentration of 50,926 ppm. The dashed blue line in figure 5 is a plot of the transmission as a function of wavelength based on this CO_2 concentration resulting from the HITRAN database. Good agreement between the measured and expected results indicates the fiber sensor probe and corresponding software are working properly.

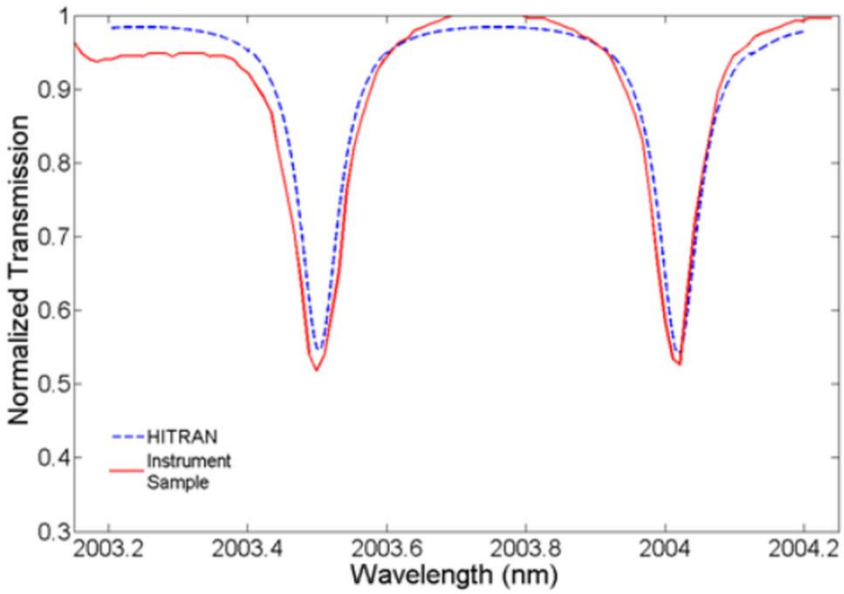

Figure 12 A plot of the normalized transmission as a function of wavelength. The solid red line represents the normalized transmission measured using one of the four probes during the release experiment. The calculated CO_2 concentration from this measured transmission was 50,926 ppm. The dashed blue line is a plot of the transmission as a function of wavelength based on this CO_2 concentration resulting from the HITRAN database.

The fiber sensor probe was operated for a fifty-eight day period, proving sub-surface CO_2 concentration measurements from each of the four probes. A plot of the CO_2 concentration as a function of time for each of the four probes between July 5 and July 9, 2012 period is shown in Figure 13. This data was collected before the subsurface CO_2

injection began thus providing background data. During this four-day period, the CO_2 concentration ranged between 1,000 and 7,000 ppm. A diurnal cycle is evident in figure 13, with a maximum CO_2 concentration occurring around 1:00 pm Mountain Daylight Time (UTC -6 hrs). There is a general decline in measured CO_2 concentrations after this time, leading to a general minimum about twelve hours later.

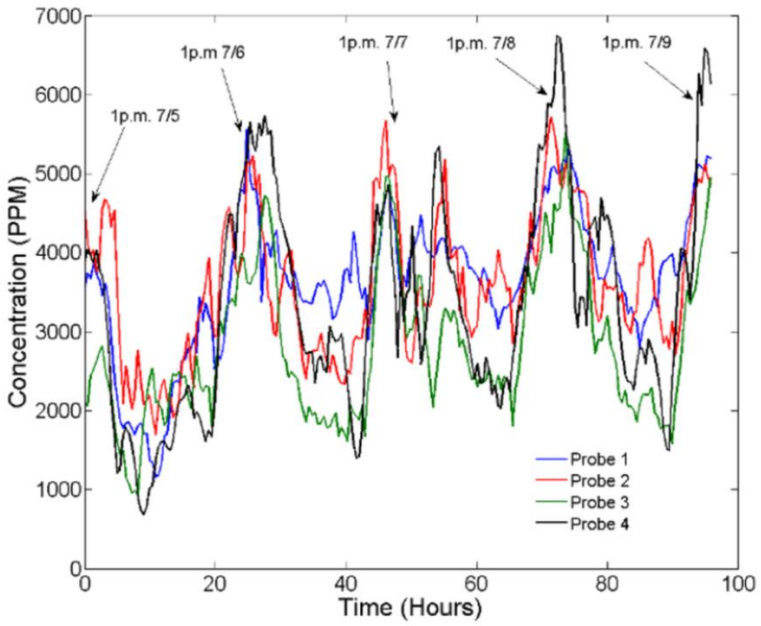

Figure 13 A plot of the CO_2 concentration as a function of time for each of the four probes measured over a four day period before the beginning July 5, 2012, before the sub-surface CO_2 release began. A diurnal cycle of subsurface CO_2 concentration is seen by each of the four probes with CO_2 concentrations ranging between 1,000 ppm and 7,000 ppm. This cycle is most likely due to microbial activity and meteorological conditions.

This diurnal cycle is related to the subsurface microbial activity as well as the surface meteorological conditions and soil moisture. Secondary peaks do occur at a couple of points in the last two days shown in Figure 13, which most likely correspond to changes

in wind speed, or air pressure due to inclement weather. These changes in surface condition can drastically affect how CO_2 rises from the soil. This data shows the each of the four fiber probes is able to monitor background CO_2 concentration levels.

A plot of the CO_2 concentration as a function of time for each of the four probes over a fifty-eight day period is shown in Figure 14. The four probes were located roughly on the corners of a rectangle with an area of about 1 m^2. The front two probes were placed closest to the pipe at a 0.5 m perpendicular distance with a maximum depth of approximately one meter. The remaining two were shifted back by about another 0.5 m. All four probes were buried at 45^o angles with respect to the horizontal surface. The CO_2 release began at 12:00 pm local time on July 10, 2012 and lasted until August 13, 2012, with the release start time and stop marked in Figure 14 with vertical lines. Data were collected twenty two days before the start of the release to ensure the instrument was able to monitor background levels. During this first twenty one days, the background CO_2 concentrations fluctuated between 1,000 ppm and 7,000 ppm showing a daily diurnal cycle. After the start of the release, the sub-surface CO_2 concentration began to rise in each of the four probes after approximately one day.

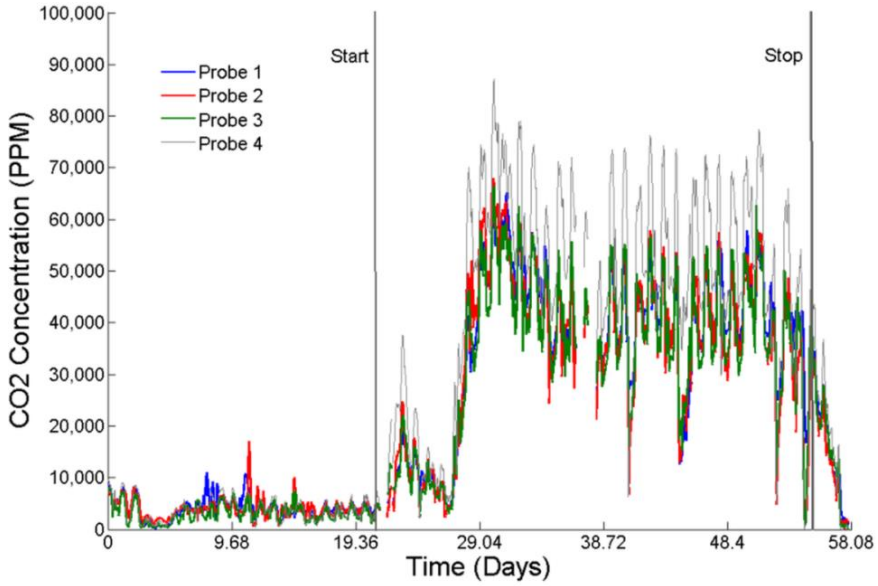

Figure 14 A plot of the sub-surface CO_2 concentration as a function of time for each of the four probes over a fifty-eight day period. The start and stop of the controlled sub-surface CO_2 release are indicated by the solid vertical lines. A rise in the sub-surface CO_2 concentration by over a factor of six over background levels indicate that the fiber sensor array can detect changes in subsurface CO_2 concentration at the level needed for geologic carbon sequestration.

This delay in the measured rise in sub-surface CO_2 concentration results from the time it takes for the CO_2 to move from the release pipe to the location of the fiber sensor probes. About two days into the release experiment, a lightning strike caused a power outage and damaged the flow controllers, causing the CO_2 flow to be stopped. This is clearly seen in the data as the drop in CO_2 concentration until about six days after the start of the release, at which time the CO_2 flow started again and each of the four probes measured a rapidly rising CO_2 concentration that reached peak levels of about 65,000 ppm for three of the four probes until the release was stopped. The other probe registered values greater than 70,000 ppm during the release. Once the release was stopped, it took

approximately three days for the subsurface CO_2 concentration values to fall back to their steady-state background levels.

Kevin Dome Deployment

During the summer of 2013 the fiber array was deployed in the field at the location known as the Kevin Dome in northern Montana.[45] The Kevin Dome is an 1800 square km subsurface, geologic formation that has both naturally occurring CO_2 and porous rock areas that would allow for storage of CO_2. In order to test the viability of carbon sequestration the naturally occurring CO_2 will be pumped from a production well along a 6 mile pipeline to an injection well where it will be sequestered at a depth of ~4000 ft.

The fiber sensor array was deployed at a point at the Kevin Dome field site and allowed to collect surface background data over seventeen nights during July and August. Due to a lack of constant electric power to run the system at the remote location, the array was operated intermittently for several hours per day. Figure 15 shows the measured CO_2 concentrations from the fiber array at the Kevin Dome field site for the four probes. Because the system was operated for smaller intervals instead of a continual 24-hour cycle, the measured CO_2 concentrations were averaged for each nightly interval during which the instrument was operating; the nightly average for each probe was plotted against each night of operation. These background measurements show similar concentrations to the measurements taken at the ZERT site the year before indicating a typical background level. The overall average for the CO_2 concentration does seem

slightly elevated, especially for night time operation when microbial activity is expected to decline and reduce sub-surface CO_2. This change in measured CO_2 may be due to a higher transmission voltage noise during the Kevin Dome deployment, due to a decrease in laser power and stability as was previously discussed. This means that the instrument was most likely measuring near the overall noise floor of ~5000 ppm. Reduction of system noise and the continual monitoring of subsurface CO_2 levels through a variety of techniques will be of interest as the actual transport and sequestering of CO_2 takes place over the life of the project.

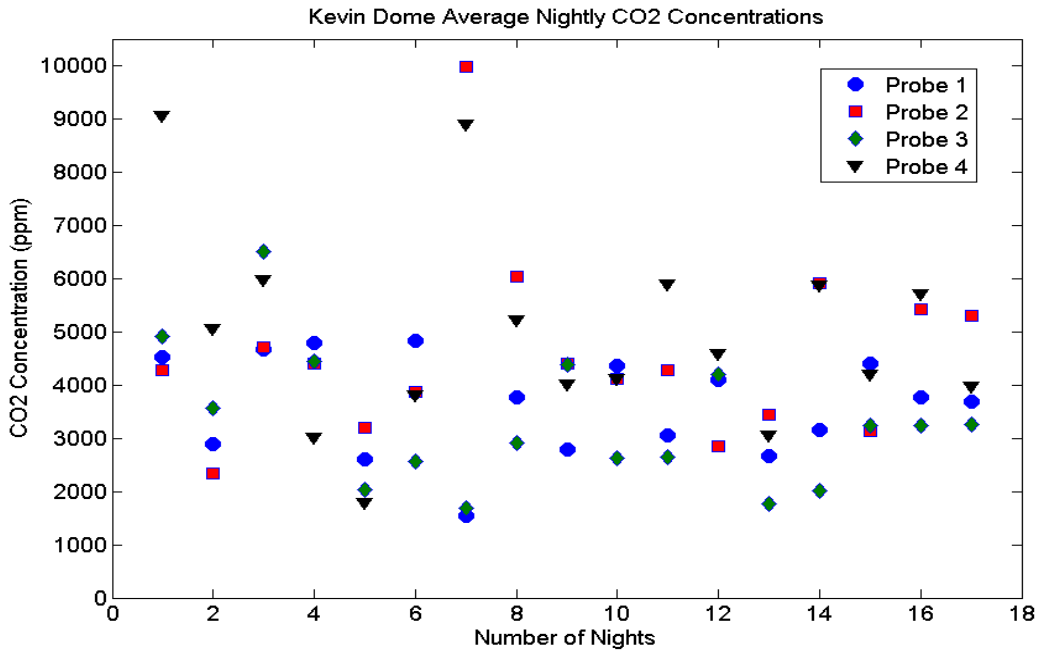

Figure 15 Plots of the background CO_2 measured during the Kevin Dome deployment.

CONCLUSION

A fiber optic sensor array for sub-surface CO_2 concentration measurements has been demonstrated at the ZERT controlled sub-surface release facility over a fifty eight day period. This 1 x 4 fiber sensor array utilizing a send/call configuration uses a single tunable DFB laser and fiber optic components to make sub-surface CO_2 concentration measurements based on integrated path differential absorption techniques. This instrument was successfully deployed over a fifty-eight day period measuring background CO_2 concentrations over twenty one days, measuring the changing sub-surface CO_2 concentrations in each of the four probes resulting from a thirty four day sub-surface controlled release, and finally monitoring the relaxation back to background levels for the three days after the injection was stopped. Background CO_2 concentrations ranged between 1,000 ppm and 7,000 ppm while the release was designed to mimic the conditions needed for successful geologic sequestration site monitoring with concentrations ranging over 70,000 ppm.

The 1 x 4 fiber optic sensor array can be scaled in a cost effective manner for monitoring larger areas. In-line fiber optic switches based on the same technology used by the 1 x 4 switch employed in this demonstration instrument are available in a number of geometries with up to 50 output ports. The part count for the expensive components including the DFB laser, detectors, and fiber optic switch does not increase as the number of probes increases and the probes have been designed to be made inexpensively. This allows the fiber sensor array to be scaled inexpensively with the added benefit that the

fiber probes can be placed as needed and easily moved providing for a reconfigurable sensor.

The fiber sensor array is currently used for sub-surface CO_2 detection. The ability to monitor other sub-surface gases including methane (CH_4) and oxygen (O_2) can provide process based information that can help determine the origin of the CO_2 [44]. For example, if photosynthesis is occurring, the ratio of the change in CO_2 will be related to the ratio of the change in O_2. The ability to monitor other soil gasses with a similar geometry can be incorporated through adding tunable DFB lasers at the appropriate wavelengths and using wavelength division multiplexers to allow for spectroscopy of multiple species in a single probe. Future research efforts may be aimed at achieving this goal.

REFERENCES CITED

[1] Scripps CO_2 Program (Scripps), 2007. Monthly average carbon dioxide concentration.
http://scrippsco2.ucsd.edu/graphics_gallery/mauna_loa_record/mauna_loa_record.html, Scripps Institute of Oceanography.

[2] P. Tans and R. Keeling, "Trends in atmospheric carbon dioxide," NOAA/ESRL & Scripps
Institute of Oceanography, http://www.esrl.noaa.gov/gmd/ccgg/trends/ , January 2012.

[3] Masarie, K. and Tans, P.P., "Extension and integration of atmosphere carbon dioxide data into a globally consistent measurement record", Journal of Geophysical Research, 100:11593–11610, June 1995.

[4] Tans, P.P., " How can global warming be traced to CO_2?", Scientific American, 295(6):124, Dec 2006.

[5] Scheffer, M., Brovkin, V. and Cox, P.M., "Positive feedback between global warming and atmospheric CO_2 concentration inferred from past climate change", Geophysical Research Letters, 33(L10702), 2006.

[6] Raupach, M.R., Marland, G., Ciais, P., Le Quere, C., Canadell, J.G., Klepper, G. and Field, C.B., "Global and regional drivers of accelerating CO_2 emission", Proceedings of the National Academy of Sciences, v104, 10,288-10,293, June 2007.

[7] IPCC (2007) Climate Change 2007: Impacts, Adaptation and Vulnerability. Contributions of Working Group II to the Fourth Assessment Report of the Intergovernmental Panel on Climate Change, M. L. Parry, O. F. Canziani, J. P. Palutikof, P. J. van der Linden, and C. E. Hanson, Eds. Cambridge University Press, Cambridge, UK, 976 pp.

[8] Karl T. R., Melillo, J.M. and Peterson, T.C., (Eds.), "Global Climate Change Impacts on the United States", Cambridge University Press, Cambridge, United Kingdom, 2009

[9] Alcamo, J. and Kreileman, G.J.J., "Emission scenarios and global climate protection", Global Environmental Change, 6(4):305–334, 1996.

[10] Climate Change 2001. Synthesis Report. A Contribution of Working Groups I, II, and III to the Third Assessment Report of the Intergovernmental Panel on Climate Change, Edited by R.T. Watson, Cambridge University Press, Cambridge, U.K., 2001.

[11] Hansen, J., "Defusing the global warming time bomb", Scientific American, 290(3):68, 2004.

[12] Norby, R.J. and Luo, Y., "Evaluating ecosystem responses to rising atmospheric CO_2 and global warming in a multi-factor world", New Phytologist, 162(2):281–293, 2006.

[13] Tans, P.T., "Trends in atmospheric carbon dioxide", National Oceanic & Atmospheric Administration, 17, April 2006.

[14] Vinnikov, K.Y. and Grody, N.C., "Global warming trend of mean tropospheric temperature observed by satellites", Science, 302:269–272, 10 October 2003.

[15] Houghton, R. A., "Balancing the Global Carbon Budget", Annu. Rev. Earth Plant. Sci., 2007.35:313-347), 2007

[16] Climate Change 2001 – Mitigation. The Third Assessment Report of the Intergovernmental Panel on Climate Change. Edited by B. Metz, O. Davidson, R. Swart, and J. Pan, Cambridge University Press, Cambridge, U.K., 2001.

[17] Herzog, H.J., "What future for carbon capture and sequestration?", American Chemical Society, 35(7):148–153, April 2001.

[18] Intergovernmental Panel on Climate Change Special Report on Carbon Dioxide Capture and Storage, Edited by B. Metz, O. Davidson H. de Coninck, M. Loos, and L. Meyer, Cambridge University Press, Cambridge, U.K., 2005.

[19] Lawrence Berkeley National Laboratory, "An Overview of Geologic Sequestration of CO2", ENERGEX'2000: Proceedings of the 8th International Energy Forum. Las Vegas, NV, July 2000.

[20] Xu, T., CO_2 geological sequestration. Lawrence Berkeley National Laboratory, Paper LBNL-56644 JArt, November 18, 2004.

[21] Li, Z., Dong, M., Li, S. and Huang, S., "CO_2 sequestration in depleted oil and gas reservoirs-caprock characterization and storage capacity", Energy conservation and Management, 47:1372–1382, 2006.

[22] Torp, T.A., Gale, J., "Demonstrating storage of CO_2 in geologic reservoirs: The Sleipner and SACS projects", Energy, 29, 1361-1369, 2004.

[23] Whittaker, S.G., Kreis, K., Davis, T.L., Hajnal, Z., Heck, T., Penner, L., Qing, H. and Rostron, B., "Characterizing the geologic container at the Weyburn Field for subsurface CO2 storage associated with enhanced oil recovery", Proceedings of the Diamond Jubilee convention of the Canadian Society of Petroleum Geologists, 2002.

[24] Whittaker, S.G., "Geological storage of greenhouse gases: The IEA Weyburn CO2 monitoring and storage project", Canadian Society of Petroleum and Geologists Reservoir, 31(8):9, Sep 2004.

[25] Lityski, J. T., Plasynski, S., McIlvried, H.G., Mahoney, C. and Srivastava, R.D., "The United States Department of Energy's Regional Carbon Sequestration Partnerships Validation Phase", Environment International, 34, 127-138, 2008

[26] Repasky, K.S., Humphries, S. and Carlsten, J.L., "Differential Absorption Measurements of Carbon Dioxide Using a Temperature Tunable Distributed Feedback Diode Laser", Review of Scientific Instruments, 77, 113107, 2006.

[27] Benson, S.M., Gasperikova, E. and Hoversten, G.M., "Monitoring protocols and life-cycle costs for geologic storage of carbon dioxide", Proceedings of the 7th International conference on greenhouse Gas control Technologies (GHGT-7), pages 1259–1266, 2005.

[28] Wilson, E.J., Friedmann, S.J. and Pollak, M.F., "Research and Development: Incorporating Risk, Regulation, and Liability for Carbon Capture and Sequestration", Environmental Science Technology, 41, 5945-5952, 2007

[29] Barr, J.L., Humphries, S.D., Nehrir, A.R., Repasky, K.S., Dobeck, L.M., Carlsten, J.L., and Spangler, L.H., "Laser Based Carbon Dioxide Monitoring Instrument Testing During a Thirty Day Controlled Underground Carbon Release Field Experiment", The International Journal of Greenhouse Gas Control, Volume:5, Issue:1, 2011.

[30] Lewicki, J.L., Oldenburg, C.M., Dobeck, L. and Spangler, L., "*Surface CO_2 leakage during the first shallow subsurface CO_2 release experiment"*, LBNL 63528. Geophysical Research Letters, 34 (L24402, doi: 101029/2007GL302047), 2008.

[31] Lewicki, J.L, Hilley, G.E., Fischer, M.L., Pan, L., Oldenburg, C.M., Dobeck, L. and Spangler, L., "*Eddy covariance observations of surface leakage during shallow subsurface CO_2", Journal* of Geophysical Research - Atmospheres, submitted, June, 2008.

[32] Baldocchi, D.D., "Assessing the eddy covariance technique for evaluating carbon dioxide exchange rates of ecosystems: past, present, and future", Global Change Biology, 9:479-492, 2003.

[33] Billesbach, D.P., Fischer, M.L., Torn, M.S. and Berry, J.A., "A portable eddy covariance system for measurement of ecosystem-atmosphere exchange of CO_2, water vapor, and energy", Journal of Atmospheric and Oceanic Technology, 21:639-650, 2004.

[34] Weldon, V., Phelan P. and Hegarty, J., "Methane and Carbon Dioxide Sensing Using A DFB Laser Diode Operating at 1.64μm", Electronics Letters, Volume: 29, Issue: 6,1993.

[35] Yu, R., Wu, W., Xia, N., Geng, H. and Liu, M., "Real-time Carbon Dioxide Emission Monitoring System Based on Participatory Sensing", Fourth International Workshop on Advanced Computational Intelligence. Wuhan, Hubei, China; October 19-21, 2011.

[36] Phelan, R., Lynch, M., Donegan, J.F. and Weldon, V., "Investigation of a Strongly Gain Coupled DFB Laser Cascade for Simultaneous Multigas Sensing", IEEE Proceedings – Volume:150, Issue: 2, 2003

[37] Kosterev, A.A., Dong, L., Thomazy, D., Tittel, F.K., Pavlovsky, I. and Romanak, K., "Portable Spectroscopic Carbon Dioxide Monitor for Carbon Sequestration Applications", Lasers and Electro-optics, 2009, and Conference on Quantum Electronics and Laser Science, CLEO/QELS 2009.

[38] Ksendzov, A., Forouhar, S., Briggs, R.M., Frez, C., Franz, K.J., Bagheri, M., " Linewidth Measurement of High Power Diode Laser at 2 μm for Carbon Dioxide Detection", Electronics Letters, Volume:48, Issue: 9, 2012.

[39] Agiltron, Lightbend 1 x N Broadband Fiber Optic Switch, http://agiltron.com/pdfs/lb% 201xn%20broad%20bend.pdf , December, 2013.

[40] Humphries, S.D., Nehrir, A.R., Keith, C.J., Repasky, K.S., Dobeck, L.M., Carlsten, J.L., and Spangler, L.H., "Testing Carbon Sequestration Site Monitoring Instruments Using a Controlled Carbon Dioxide Release Facility", Applied Optics, 47, 548-555, 2008.

[41] Spangler, L.H., Dobeck, L.M., Repasky, K., Nehrir, A., Humphries, S., Barr, J.L., Keith, C., Shaw, J., Rouse, J., Cunningham, A., Benson, S., Oldenburg, C.M., Lewicki, J.L., Wells, A., Diehl, R., Strazisar, B., Fessenden, J., Rahn, T., Amonette, J., Barr, J., Pickles, W., Jacobson, J., Silver, E., Male, E., Rauch, H., Gullickson, K., Trautz, R., Kharaka, Y., Birkholzer, J. and Wielopolski, L., "A controlled field pilot in Bozeman, Montana, USA, for testing near surface CO_2 detection techniques and transport models" Environmental Earth Science, 2010, 60:227-239, doi:12.107/s12665-009-0400-2.

[42] Rothman, L.S., Barbe, A., Benner, D.C., Brown, L.R., Camy-Peyret, C., Carleer, M.R., Chance, K., Clerbaux, C., Dana, V., Devi, V.M., Fayt, A., Flaud, J.M., Gamache, R.R., Goldman, A., Jacquemart, D., Jucks, K.W., Lafferty, W.J., Mandin, J.Y., Massie, S.T., Nemtchinova, V., Newnham, D.A., Perrin, A., Rinsland, C.P., Schroeder, J., Smith, K.M., Smith, M.A.H., Tang, K., Toth, R.A., Vander Auwera, J., Varanasi, P. and

Yoshino, K.,"THE HITRAN molecular spectroscopic database,"J. *Quant. Spectrosc. Radiat. Transfer* **82,** 5–44, 2003.

[43] Optical Remote Sensor Laboratory, Dr. Joseph Shaw, Montana State University, Electrical and Computer Engineer Department. http://orsl.eps.montana.edu/weather/

[44] Romanak, K. D., Bennett, P. C., Yang, C., and Hovorka, S.D., "Process-based approach to CO_2 leakage detection by vadose zone gas monitoring at geologic CO_2 storage sites", *Geophys. Res. Lett.*, 39, L15405, doi:10.1029/2012GL052426, 2012.

[45] http://www.bigskyco2.org/research/geologic/kevinstorage

APPENDICES

APPENDIX A

INSTRUMENT SCHEMATICS

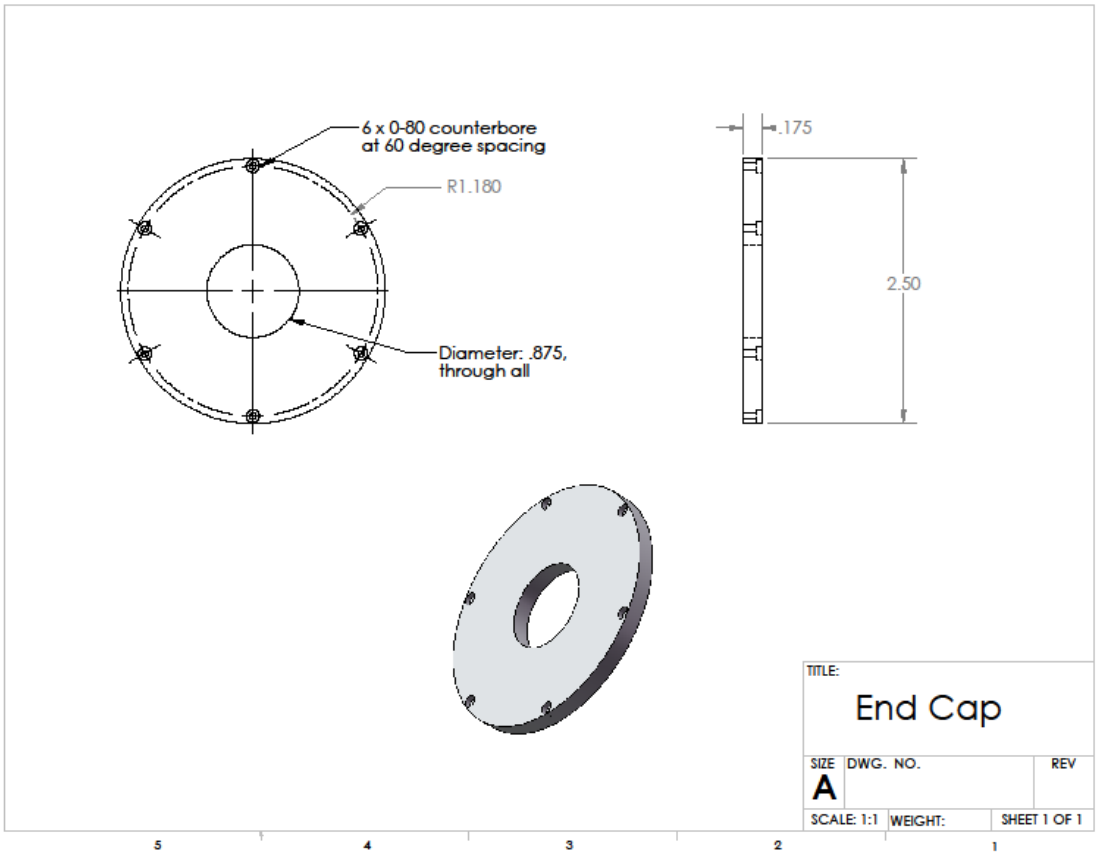
6 x 0-80 counterbore
at 60 degree spacing
R1.180
Diameter: .875,
through all
.175
2.50
TITLE:
End Cap
SIZE
A
DWG. NO.
REV
SCALE: 1:1
WEIGHT:
SHEET 1 OF 1
5
4
3
2
1

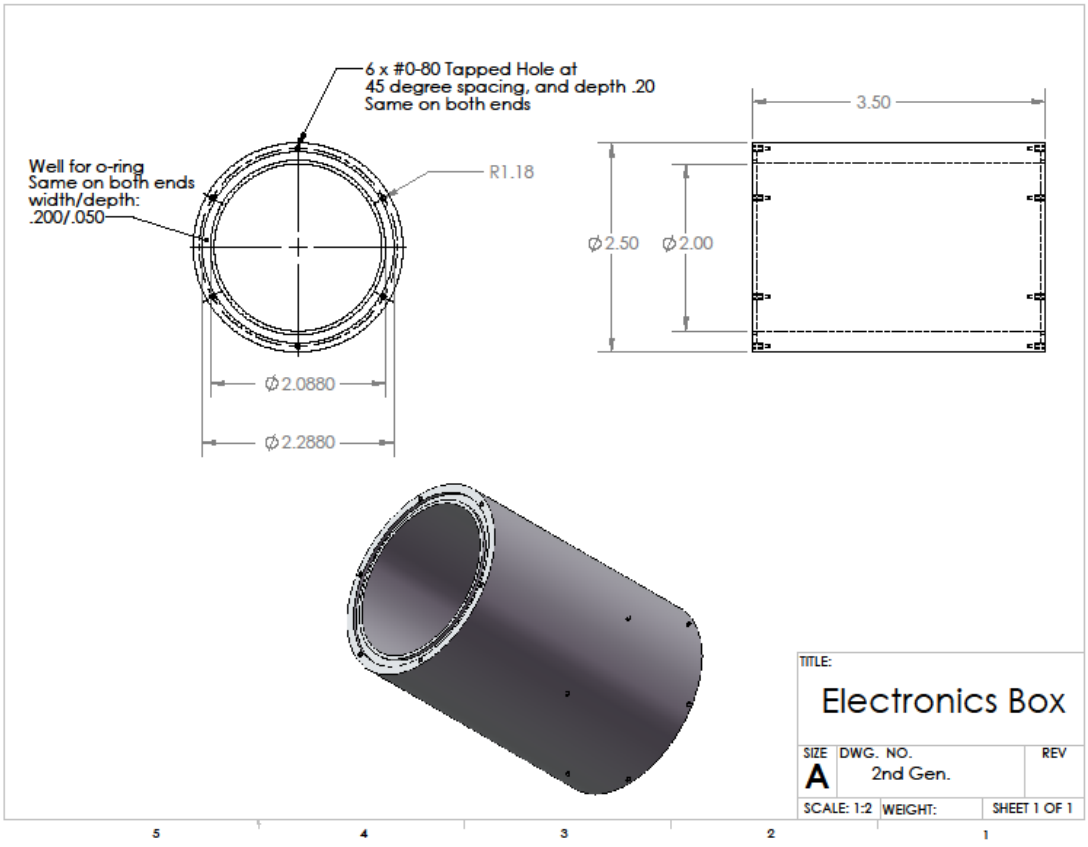
6 x #0-80 Tapped Hole at
45 degree spacing, and depth .20
Same on both ends
Well for o-ring
Same on both ends
width/depth:
.200/.050
R1.18
Ø2.0880
Ø2.2880
3.50
Ø2.50
Ø2.00
TITLE:
Electronics Box
SIZE
A
DWG. NO.
2nd Gen.
REV
SCALE: 1:2
WEIGHT:
SHEET 1 OF 1
5
4
3
2
1

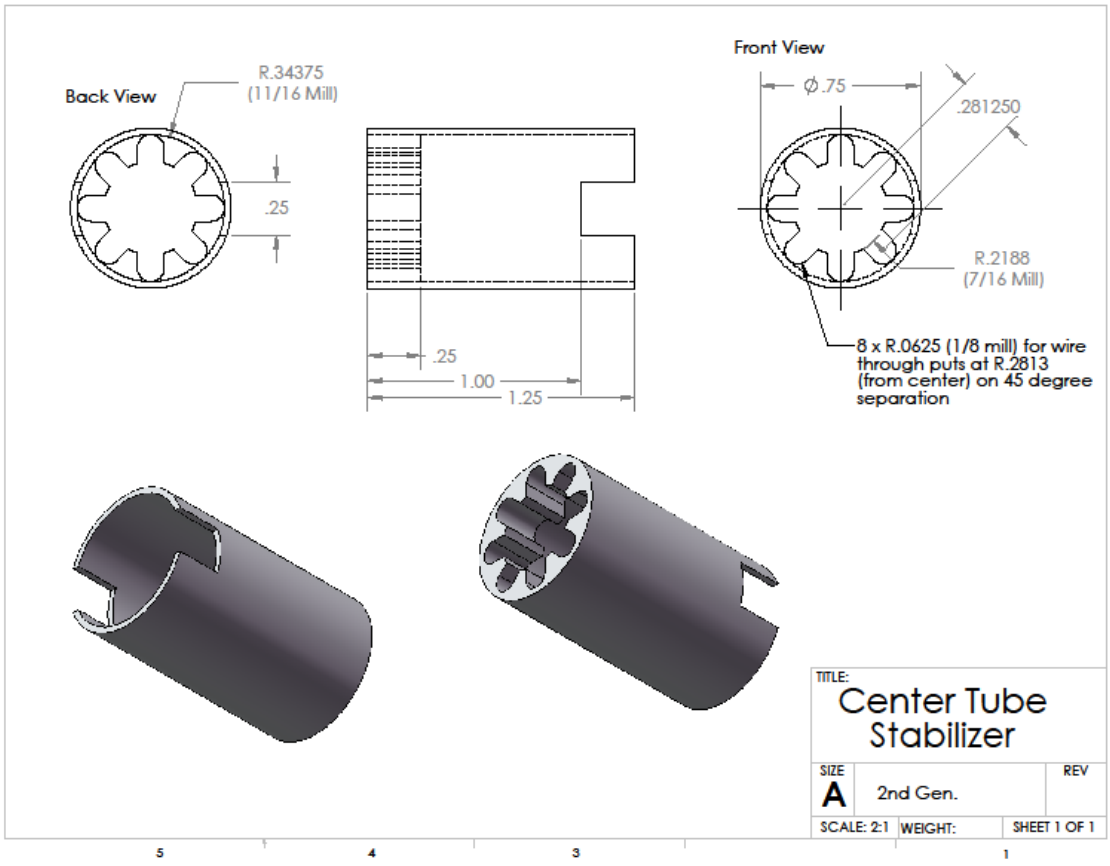
Back View
R.34375
(11/16 Mill)
.25
.25
1.00
1.25
Front View
Ø.75
.281250
R.2188
(7/16 Mill)
8 x R.0625 (1/8 mill) for wire through puts at R.2813 (from center) on 45 degree separation
TITLE:
Center Tube Stabilizer
SIZE
A
2nd Gen.
REV
SCALE: 2:1
WEIGHT:
SHEET 1 OF 1
5
4
3
1

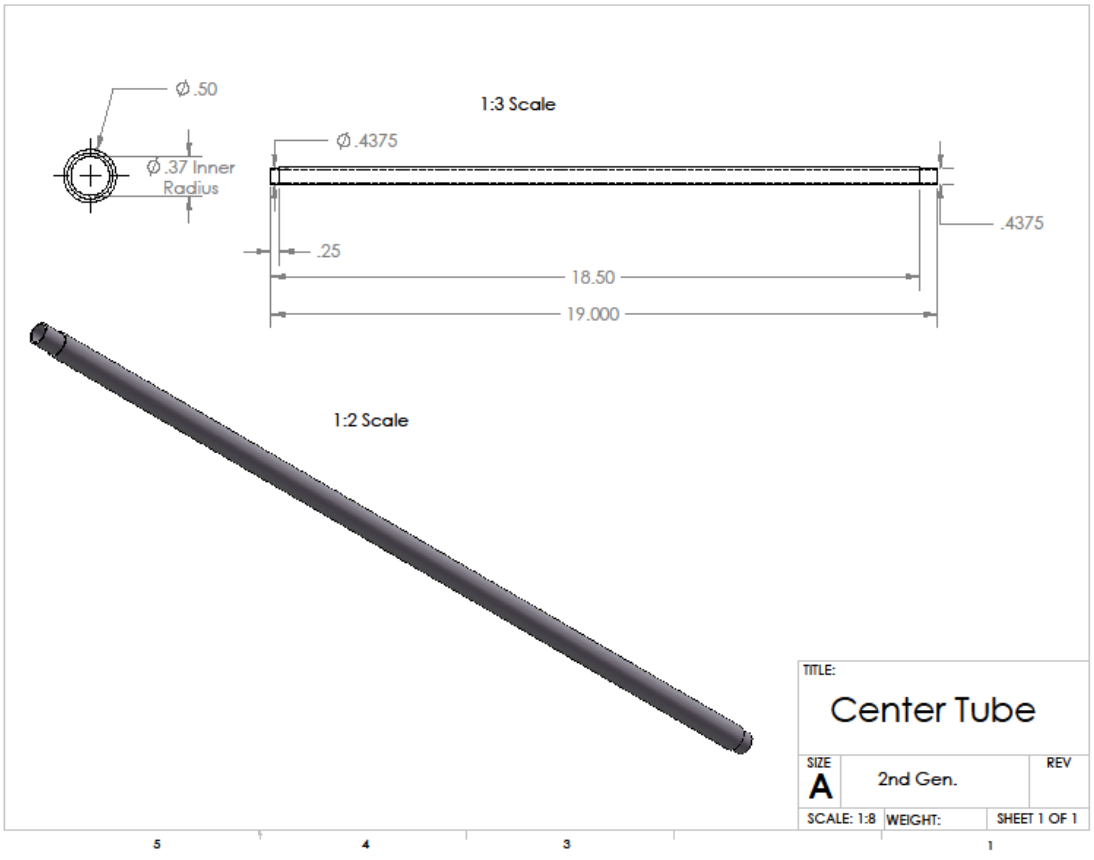
Ø.50
Ø.37 Inner Radius
1:3 Scale
Ø.4375
.4375
.25
18.50
19.000
1:2 Scale
TITLE:
Center Tube
SIZE
A
2nd Gen.
REV
SCALE: 1:8
WEIGHT:
SHEET 1 OF 1
5
4
3
1

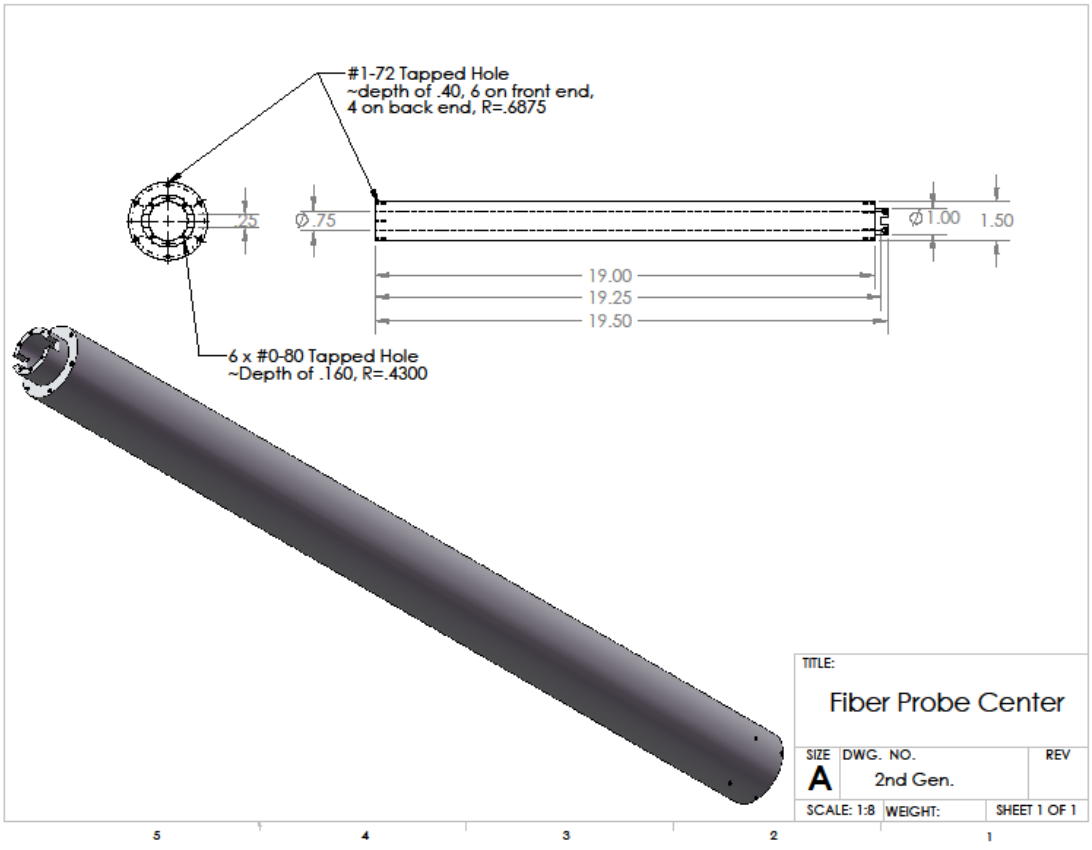
#1-72 Tapped Hole
~depth of .40, 6 on front end,
4 on back end, R=.6875
.25
Ø.75
Ø1.00
1.50
19.00
19.25
19.50
6 x #0-80 Tapped Hole
~Depth of .160, R=.4300
TITLE:
Fiber Probe Center
SIZE
A
DWG. NO.
2nd Gen.
REV
SCALE: 1:8
WEIGHT:
SHEET 1 OF 1
5
4
3
2
1

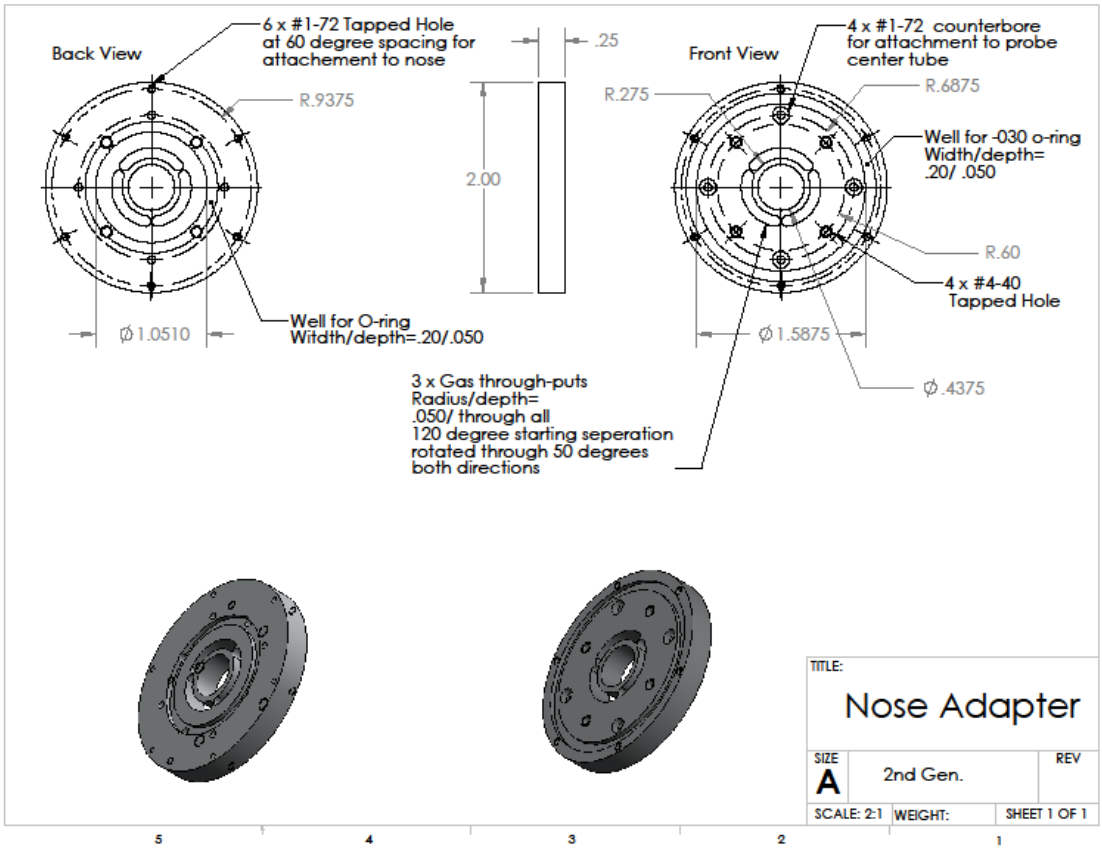
Back View
6 x #1-72 Tapped Hole
at 60 degree spacing for
attachement to nose
R.9375
Well for O-ring
Witdth/depth=.20/.050
Ø1.0510
.25
2.00
Front View
4 x #1-72 counterbore
for attachment to probe
center tube
R.275
R.6875
Well for -030 o-ring
Width/depth=
.20/ .050
R.60
4 x #4-40
Tapped Hole
Ø1.5875
Ø.4375
3 x Gas through-puts
Radius/depth=
.050/ through all
120 degree starting seperation
rotated through 50 degrees
both directions
TITLE:
Nose Adapter
SIZE
A
2nd Gen.
REV
SCALE: 2:1
WEIGHT:
SHEET 1 OF 1
5
4
3
2
1

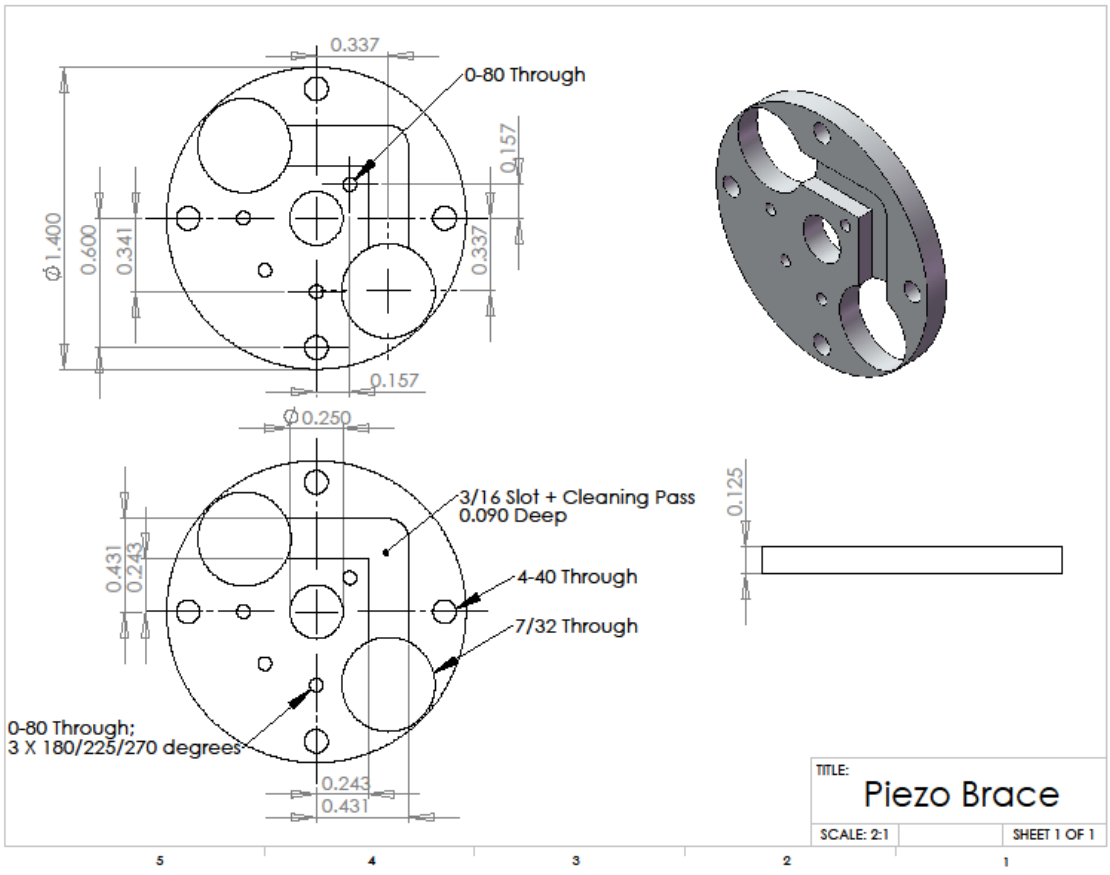
0.337
0-80 Through
0.157
Ø1.400
0.600
0.341
0.337
0.157
Ø0.250
3/16 Slot + Cleaning Pass
0.090 Deep
0.125
0.431
0.243
4-40 Through
7/32 Through
0-80 Through;
3 X 180/225/270 degrees
0.243
0.431
TITLE:
Piezo Brace
SCALE: 2:1
SHEET 1 OF 1
5
4
3
2
1

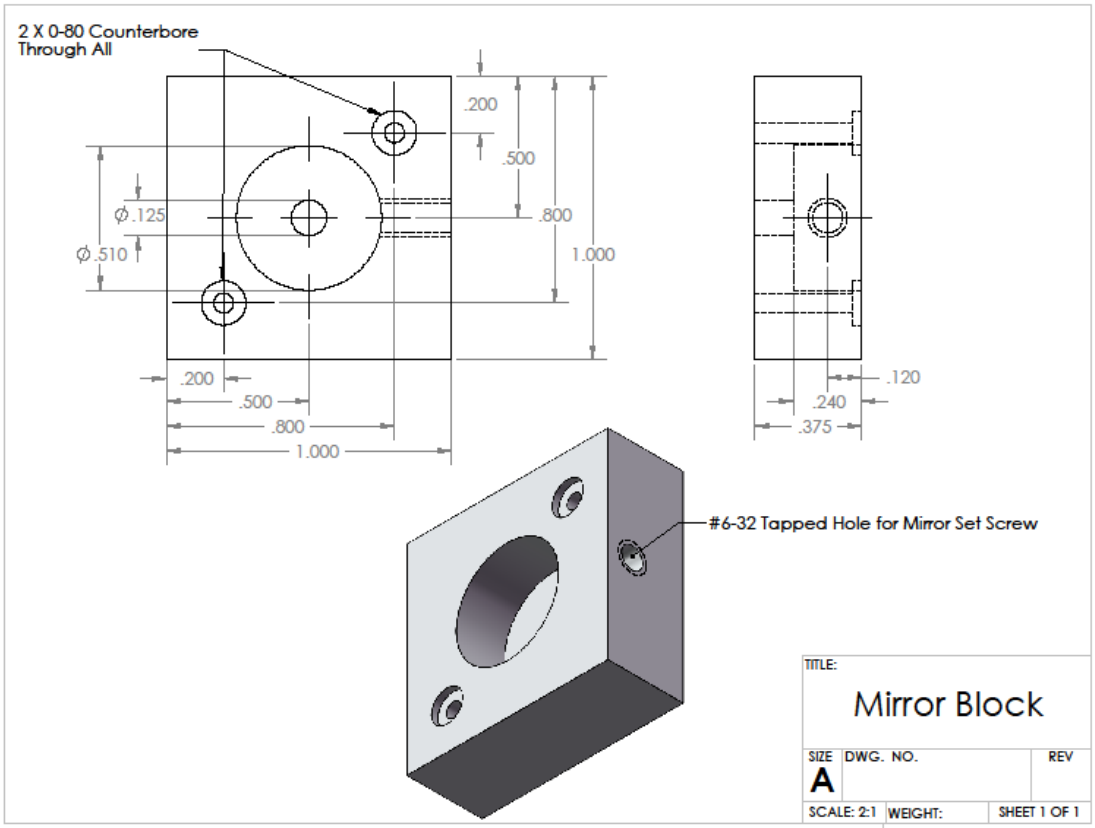
2 X 0-80 Counterbore
Through All
.200
.500
.800
1.000
Ø.125
Ø.510
.200
.500
.800
1.000
.120
.240
.375
#6-32 Tapped Hole for Mirror Set Screw
TITLE:
Mirror Block
SIZE
A
DWG. NO.
REV
SCALE: 2:1
WEIGHT:
SHEET 1 OF 1

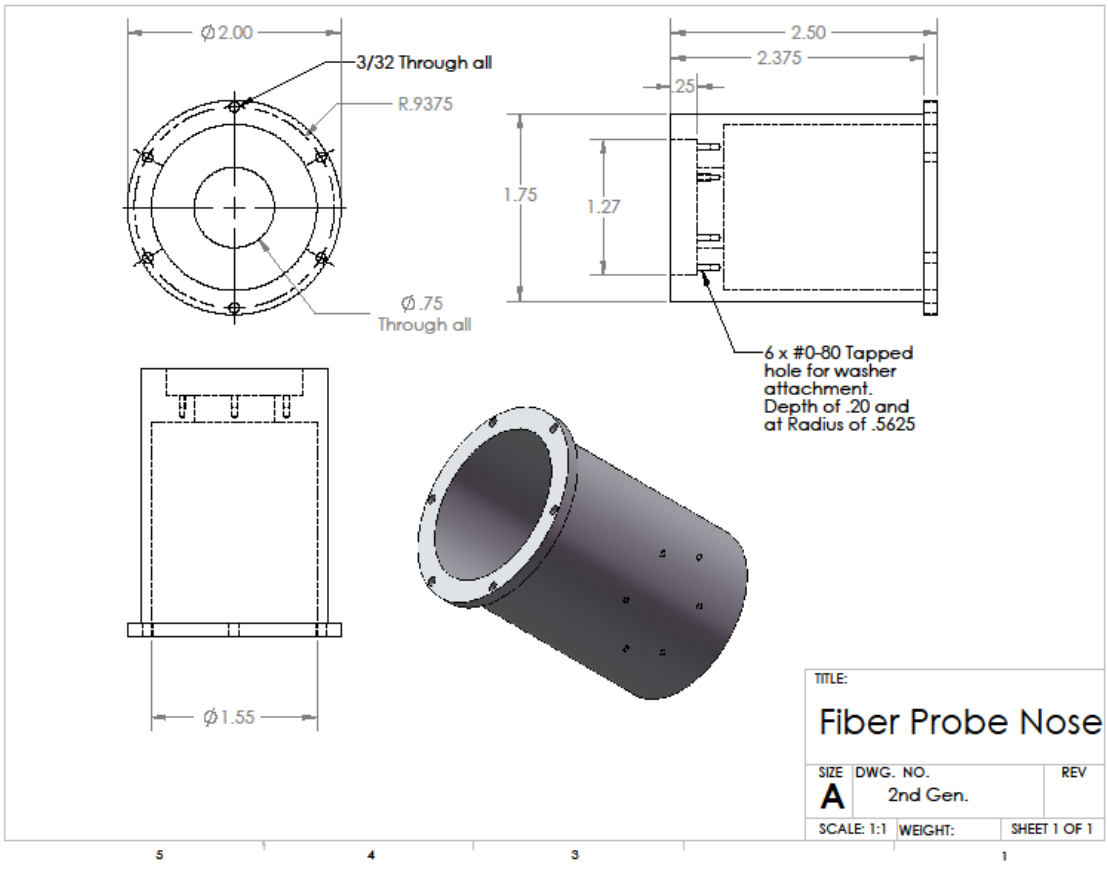
Ø2.00
3/32 Through all
R.9375
Ø.75
Through all
2.50
2.375
.25
1.75
1.27
6 x #0-80 Tapped
hole for washer
attachment.
Depth of .20 and
at Radius of .5625
Ø1.55
TITLE:
Fiber Probe Nose
SIZE
A
DWG. NO.
2nd Gen.
REV
SCALE: 1:1
WEIGHT:
SHEET 1 OF 1
5
4
3
1

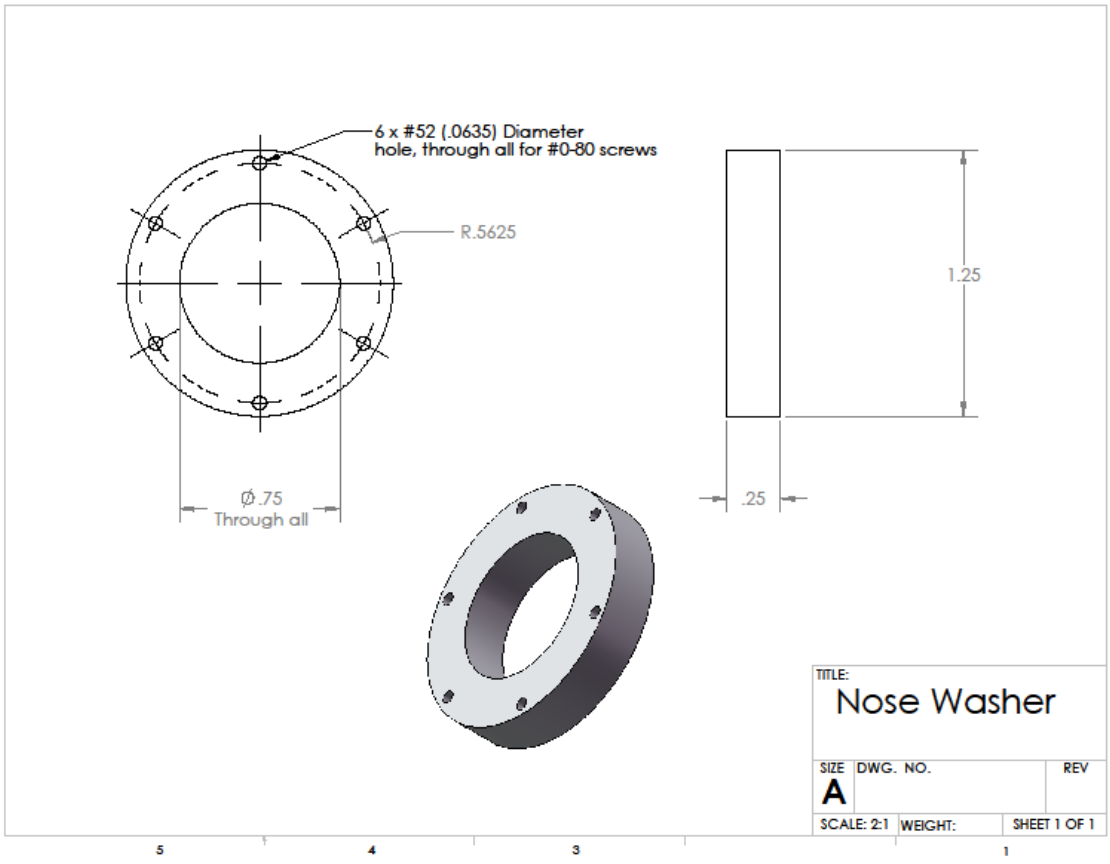
6 x #52 (.0635) Diameter
hole, through all for #0-80 screws
R.5625
Ø.75
Through all
1.25
.25
TITLE:
Nose Washer
SIZE
A
DWG. NO.
REV
SCALE: 2:1
WEIGHT:
SHEET 1 OF 1
5
4
3
1

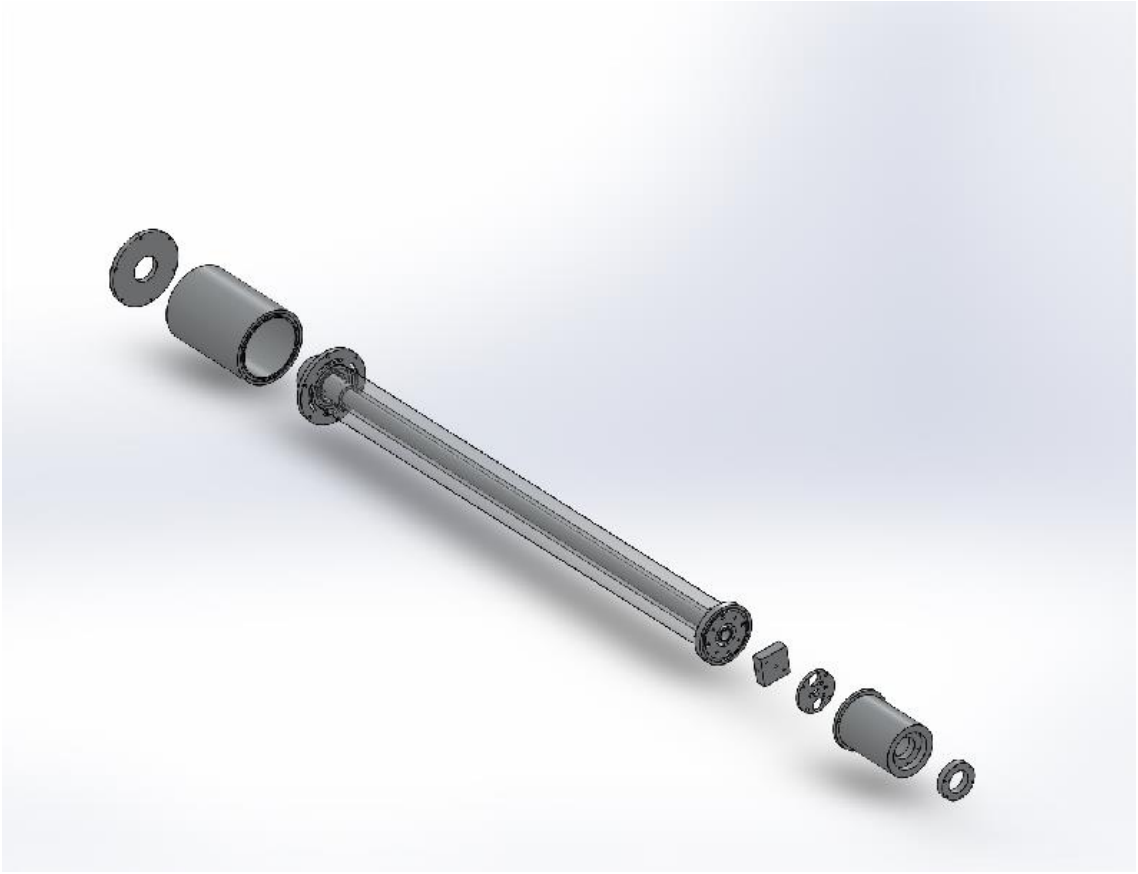

Exploded Assembly

APPENDIX B

PROGRAMMING FOR DATA COLLECTION AND ANALYSIS

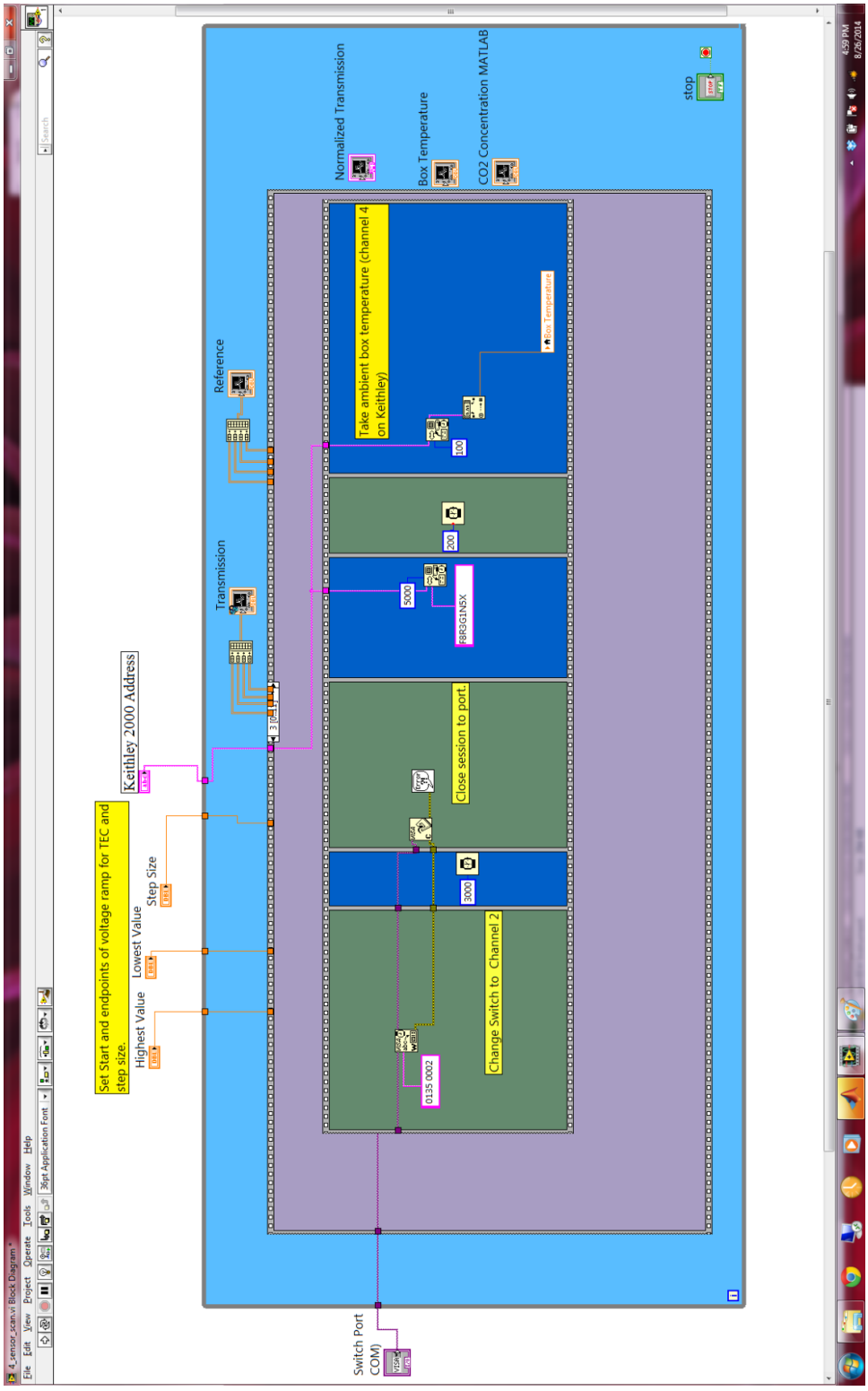
Switch Port COM)
Set Start and endpoints of voltage ramp for TEC and step size.
Highest Value
Lowest Value
Step Size
Keithley 2000 Address
Transmission
Reference
Change Switch to Channel 2
Close session to port.
Take ambient box temperature (channel 4 on Keithley)
Normalized Transmission
Box Temperature
CO2 Concentration MATLAB
stop

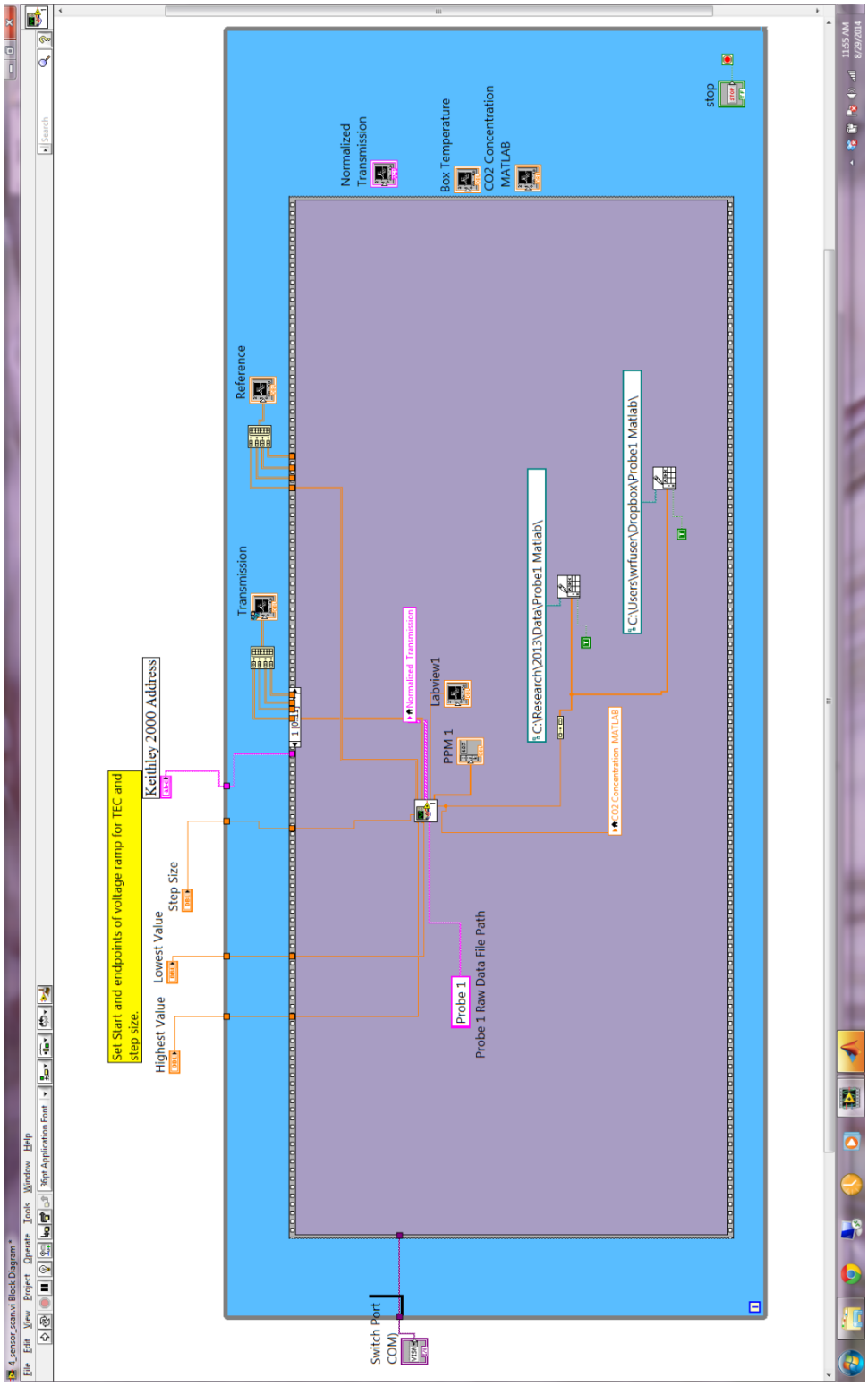
Set Start and endpoints of voltage ramp for TEC and step size.
Keithley 2000 Address
Lowest Value
Step Size
Highest Value
Switch Port COM
Transmission
Reference
Normalized Transmission
Box Temperature
CO2 Concentration MATLAB
stop
Labview1
PPM 1
Probe 1
Probe 1 Raw Data File Path
C:\Research\2013\Data\Probe1 Matlab\
C:\Users\wrfuser\Dropbox\Probe1 Matlab\

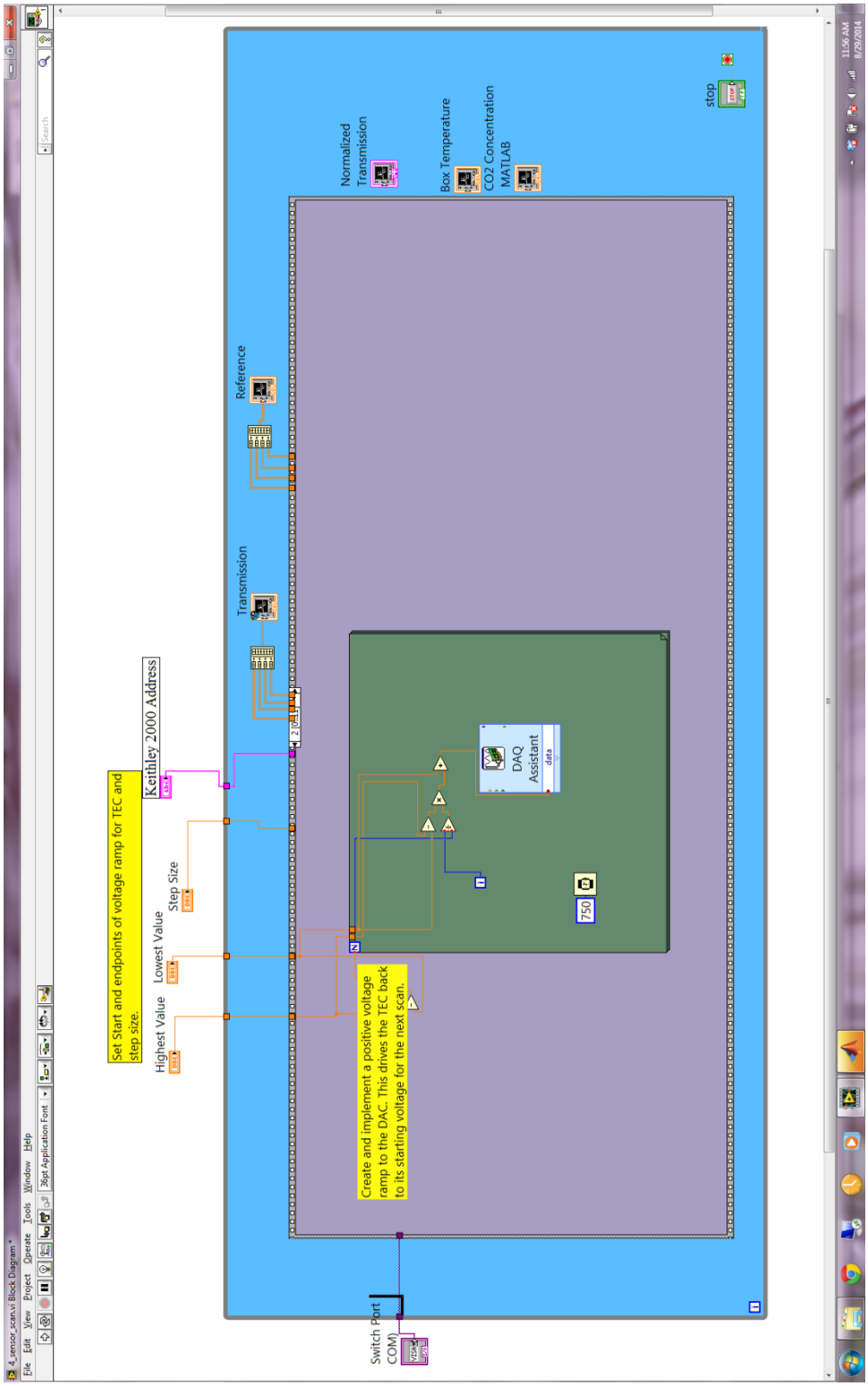
4_sensor_scan.vi Block Diagram *
File Edit View Project Operate Tools Window Help
36pt Application Font
Search
Set Start and endpoints of voltage ramp for TEC and step size.
Keithley 2000 Address
Lowest Value
Step Size
Highest Value
Transmission
Reference
Normalized Transmission
Box Temperature
CO2 Concentration MATLAB
stop
DAQ Assistant
data
750
Create and implement a positive voltage ramp to the DAC. This drives the TEC back to its starting voltage for the next scan.
Switch Port (COM)
11:56 AM
8/29/2014

```
Coding for the concentration and error
% First, retrieve the index file with all scan timestamps for specific
probe and load into
  % matlab
        %C:\Research\2013\Data\Probe #\Probe #_Index.dat  -actual file
  Probe = 'Probe 1';  %set the probe # you are working with
  date = '1-16 to 1-26'; %set the date range you are working with
  dT=.05; % set the trasmission error...this will change depending on
the probe
  time =.25:.25:272.75;  %set the time vector ".8 hours between each
probe scan" for my scans - this number can change so beware
  path = strcat('C:\Research\2014\Data\',Probe,'\',Probe,'_Index.dat');
%make sure you set your 'year' correctly
  index_all = load(path);



  %Now create new index file with iterations of 100 (this number is
  %arbitrary and simply derterminines how many points you wish to do an
error
  %analysis on)

  y = size(index_all,1);
       month_day = zeros(y,1); %y is the total number of scans
       hour_min_sec = zeros(y,1);

  month_day(:,1) = index_all(:,1); %makes two separate files containing
  hour_min_sec(:,1) = index_all(:,2);  %the month/day/year and
Hr/Min/Sec from the index file
  Conc = zeros(size(index_all,1),1); %initialize the arrays for the
concentration and the errors
  C = zeros(size(index_all,1),1);
  dCT = zeros(size(index_all,1),1);
  %% BEGIN THE CONCENTRATION CALCULATION FOR THE 2 LINES AND TAKE THEIR
AVERAGE

 for q = 1:size(index,1) %for each scan (100 points) a single
concentration and error will be calculated
      MDY = sprintf('%08d',month_day(q,1));  % creating file path to
load scans
      HMS = sprintf('%06d',hour_min_sec(q,1));

            % C:\Research\2013\Data\Probe #\MDY\HMS
      file_name =
strcat('C:\Research\2014\Data\',Probe,'\',MDY,'\',HMS,'.dat');
      %file_name = strcat('C:\Research\2013\Data\Probe
1\','07222012\','000331.dat');
      scan_file = load(file_name);

   %file now loaded
   %first define all constants for concentration calculation

    N=2.479*10^19; %Loschmidts number (mol/cm^3*atm)
    P = .850; %pressure in atmospheres
```

```
    L = 100; %cell length in centimeters

    S(1)=1.302*10^-21;  %linestrengths (cm/mol)
    S(2)=1.332*10^-21;

    FWHM(1) = 0.1444;  %FWHM of of absorption lines
    FWHM(2) = 0.1468;

    g = zeros(1,2);
    g(1) = 1/(pi * ((FWHM(1))/2)); %lineshapes (1/cm)
    g(2) = 1/(pi * ((FWHM(2))/2));
    % Temperature factor

    Tambient = (mean(scan_file(:,5))) * (-0.0019) + 316.84;
    Treference = 296;
    Tfactor = Treference/Tambient;


    for i=1:size(scan_file,1);

        scan_file(i,6) = scan_file(i,3)/max(scan_file(:,3));

    end

    %% ------------------------------------------------------------------
----

    % Beginning data sorting to calculate concentration
    % Find indeces corresponding to peak minima

    for i = 11:38

        if i == 11
           min1 = 1;
        end

        min1 = min(min1,scan_file(i,6));

        if min1 < scan_file(i,6)
           min1index = min1index;  %#ok<ASGSL>
        else
           min1index = i;
        end
    end

    for i = 60:85

        if i == 60
           min2 = 1;
        end
```

```
        min2 = min(min2,scan_file(i,6));

        if min2 < scan_file(i,6)
           min2index = min2index;    %#ok<ASGSL>
        else
           min2index = i;
        end
    end
%%
    % Find center of maxima and corresponding
    % normalized transmission value

    for i = 1:10

        if i == 1
           max1 = scan_file(i,6);
           max1index = i;
        end

        max1 = max(max1,scan_file(i,6));

        if max1 > scan_file(i,6)
           max1index = max1index;    %#ok<ASGSL>
        else
           max1index = i;
        end
    end

    for i = 90:101

        if i == 90
           max3 = scan_file(i,6);
           max3index = i;
        end

        max3 = max(max3,scan_file(i,6));

        if max3 > scan_file(i,6)
           max3index = max3index;    %#ok<ASGSL>
        else
           max3index = i;
        end

    end
 %%
%find the maximum between the two absorption features
max2index = round((min1index + min2index)/2);


max1value = (scan_file(max1index,6) + scan_file(max1index + 1,6) + ...
                scan_file(max1index + 2,6))/3;
```

```
max2value = (scan_file(max2index - 2,6) + scan_file(max2index - 1,6) +
...
               scan_file(max2index,6)   + scan_file(max2index + 1,6) +
...
               scan_file(max2index + 2,6))/5;
max3value = (scan_file(max3index - 2,6) + scan_file(max3index - 1,6) +
...
               scan_file(max3index,6))/3;

% Build vectors of max values and indeces
x = zeros(1,3);

x(1,1) = max1index;
x(1,2) = max2index;
x(1,3) = max3index;

y = zeros(1,3);

y(1,1) = max1value;
y(1,2) = max2value;
y(1,3) = max3value;


% Build linear approximation for polyfit framework

x1 = zeros(1,x(1,3));
y1 = zeros(1,x(1,3));

        for p = x(1,1):x(1,2)

        m1 = (y(1,2) - y(1,1))/(x(1,2) - x(1,1));
        x1(1,p) = p;
        y1(1,p) = m1 * x1(1,p) + y(1,1) - m1 * x(1,1);

        end

        for p = x(1,2):x(1,3)

        m2 = (y(1,3) - y(1,2))/(x(1,3) - x(1,2));
        x1(1,p) = p;
        y1(1,p) = m2 * x1(1,p) + y(1,2) - m2 * x(1,2);

        end

T = zeros(1,2);

T(1) = scan_file(min1index,6)/y1(min1index);
T(2) = scan_file(min2index,6)/y1(min2index);

% CALCULATE CONCENTRATION
    C = zeros(1,2);
```

```
        for i = 1:2

        if T(i) < 1
           C(i) = (-log(T(i)))/(S(i) * g(i) * N * Tfactor * P * L) *
10^6;
        else
           C(i) = 0;
        end

        end

    % 2-line nonzero average concentration (PPM)

        if ~ isempty(C)
       Conc(q,1) = round(mean(nonzeros(C)));
         else
       Conc(q,1) = 0;
         end
%%this is the end of the 2-line concentation calculation
%% CALCULATING THE ERROR IN THE CONCENTRATION dC
 %now begin the error calculation to attach to each concentration value
calculated
 %Errors--- Probe 1 = .03, Probe 2 = .07, Probe 3= Probe 4 = .05 -
again
 %these  values will change as the system does
 %error in the transmission moved to first frame
 dC = zeros(1,2);

    for i = 1:2 %error for each of the absorption lines

     dC(i) = ((dT*10^6)/(S(i)*g(i)*N*Tfactor*P*L*T(i)));

    end

   dCT(q,1) = (dC(1,1) +dC(1,2))/2; %average of the error.

 end

 %% CREATING ARRAYS FOR PLOTTING THE CONCENTRATION
 % this is entirely up to you.
averaged(:,1) = filter(1,6,Conc(:,1)); %3 point running average on
concentation values
averaged(:,2) = dCT(:,1);   %error and averaged concentration in one
array "averaged" the error is in column 2
Total(:,1) = Conc(:,1);    %"Total" is the non-averaged concentrations
and errors
Total(:,2) = dCT(:,1);
%creating arrays with the error bar spacing (errordist), the errors at
each
%point (errors), and the concentration at that point (errorconc)
%Ben - August 2014 still needs work
```

```
delta =100; %this is the spacing between the errors bars you can choose

errordist = zeros(floor(length(time)/delta),1);
errors = zeros(floor(length(time)/delta),1);
errorconc = zeros(floor(length(time)/delta),1);
%% CREATING ARRAYS FOR ERROR BAR PLOTTING
p = 1:delta:floor(length(time));
    for q = 1:floor(length(time)/delta);
        errordist(q,1) = time(1,p(q));
        errors(q,1) = averaged(p(q),1);
        errorconc(q,1) = averaged(p(q),2);
    end;
    errortotal(:,1) = errors(:,1);
    errortotal(:,2) = errorconc(:,1);

%% FRAME SETS MINIMUM TO ZERO IF THE ERRORS ARE LARGER THANT HE
MEASURED VALUE
    %This sequence basically creates a vector that will not allow the
erros to go below zero
    % do this for either the entire number of files or just the ones
    % selected by delta - choose to run this frame or the next...not
both
low =zeros(length(index_all),1);
for q = 1:length(index_all)-1
   if averaged(q,1)>averaged(q,2)/2
     low(q,1)=averaged(q,2)/2;
  else low(q,1)=averaged(q,1);
    end
end

%% FRAME SETS MINIMUM TO ZERO IF THE ERRORS  ARE LARGER THAN THE
MEASURED VALUE
low =zeros(length(errortotal),1);
for q = 1:length(errortotal)
    if errors(q,1) > errortotal(q,2)/2
        low(q,1) = errortotal(q,2)/2;
    else
        low(q,1) = errortotal(q,1);
    end
end;

%% THIS FRAME ALLOWS FOR PLOTTING OF THE DATA AND THE ERRORS
%Plotting!!!

figure = errorbar(errordist,errors,low,'r');
hold on
plot(time, averaged(:,1));
figure_title= strcat(Probe,' Concentration', date,' (MATLAB)');
title(figure_title) %  --or whatever probe you are on
ylabel('PPM');
xlabel('Time (Hours)')
hold off
```

```
%%
clear;
%% ANYTHING AFTER THIS IS PROGRAMMING THAT CAN BE USED TO SAVE THE DATA
AUTOMATICALLY OR IS LEGACAY
%PROGRAMMING THAT MAY OR MAY NOT BE USEFUL.

    %saving the individual Concentrations calculated and the errors.
Also,
    %saving plots.
     %write_file_name=strcat('C:\Research\2013\7-11 to 7-
12\',Probe,'\Total_',Probe);
     %write_file_name_1=strcat('C:\Research\2013\7-11 to 7-
12\',Probe,'\averaged_',Probe);
     %write_file_name_2=strcat('C:\Research\2013\7-11 to 7-
12\',Probe,'\low_',Probe);
     %write_file_name_3=strcat('C:\Research\2013\7-11 to 7-
12\',Probe,'\time_',Probe);

%write_file_name=strcat('C:\Research\2014\',date,'\',Probe,'_variables'
);
  %figure_name=strcat('C:\Research\2014\',date,'\',Probe,'_plot');
     %dlmwrite(write_file_name, Total, delimiter, '\t');
     %dlmwrite(write_file_name_2, averaged);
 % save(write_file_name);
     %save(write_file_name_1, averaged);
     %save(write_file_name_2, low);
     %save(write_file_name_3,time);
 % saveas(figure, figure_name);
 %% extra coding
 for q = 1:length(data1)
if P1averaged(q,1)>P1averaged(q,2)/2
low(q,1)=P1averaged(q,2)/2;
else low(q,1)=P1averaged(q,1);
end
end
%%
%low2=low;
%P2averaged(:,3)=P2averaged(:,2);
figure = errorbar(data4,P4averaged(:,1),low4,P4averaged(:,3)/2);
%%title('CO2 Concentration July-Aug. 2013');
```